# EPR as a Tool to Study Isolated and Coupled Paramagnetic Centers in Coordination Compounds and Macromolecules of Biological Interest

Alberto C. Rizzi, Nicolás I. Neuman, Pablo J. González, Carlos D. Brondino*

Departamento de Física, Facultad de Bioquímica y Ciencias Biológicas, Universidad Nacional del Litoral, 3000 Santa Fe, Argentina

*To whom correspondence should be addressed. E-mail: brondino@fbcb.unl.edu.ar, Fax: + 54-32-4575221

www.fbcb.unl.edu.ar/dfbioq

**Biographical sketches**

Alberto C. Rizzi received B.S. and Ph.D. degrees from Universidad Nacional del Litoral (Argentina) and was a postdoctoral fellow at Max Planck Institute for Bioinorganic Chemistry (Germany). He is now professor in the Department of Physics in the Facultad de Bioquímica y Ciencias Biológicas at Universidad Nacional del Litoral. His research interests include the role of transition metals ions in biology and the study of bioinorganic systems as models for complex biological compounds using Electron Paramagnetic Resonance (EPR) and magnetic measurements.

Nicolás I. Neuman received B.S. and Ph.D. degrees from Universidad Nacional del Litoral, Argentina. He was a postdoctoral fellow in the Facultad de Ciencias Exactas y Naturales at Universidad de Buenos Aires, Argentina, and is now an assistant researcher and a professor in the Department of Physics in the Facultad de Bioquímica y Ciencias Biológicas at Universidad Nacional del Litoral, Argentina. His research interests include EPR of transition metal ion clusters and the development of catalysts for water oxidation.

Pablo J. González received B.S. degree from Universidad Nacional del Litoral and Ph.D. degree in Biophysical Chemistry in the Department of Chemistry in the Faculdade de Ciências e Tecnologia at Universidade Nova de Lisboa (Portugal). He had postdoctoral training in biophysical techniques applied to the study of metalloenzymes before joining as a research scientist to REQUIMTE at FCT-UNL in Portugal. He is currently a professor and a research scientist (CONICET) in the Facultad de Bioquímica y Ciencias Biológicas at Universidad Nacional del Litoral, Argentina.

Carlos D. Brondino received B.S. and Ph.D. degrees from Universidad Nacional del Litoral (Argentina). He was a postdoctoral and research fellow in the Department of Chemistry at Universidade Nova de Lisboa, Portugal. He is now a full professor, head of Department, and a research fellow of CONICET in the Department of Physics in the Facultad de Bioquímica y Ciencias Biológicas at Universidad Nacional del Litoral. His principal research interests concern the reaction mechanism of metalloenzymes involved in the biological cycles of nitrogen and sulfur and the development of EPR-based methodologies to characterize the magnetic properties of paramagnetic systems of biological interest.

From left to right: Alberto C. Rizzi, Nicolás I. Neuman, Pablo J. González, Carlos D. Brondino

**Key Topic:**

EPR Spectroscopy

**Table of Contents Text**

This microreview shows in a unified way the information that CW EPR can provide to the understanding of the electronic structure and magnetic properties of distinct types of weakly coupled paramagnetic transition metal ions present in systems of biological relevance.

**Table of Contents Graphical**

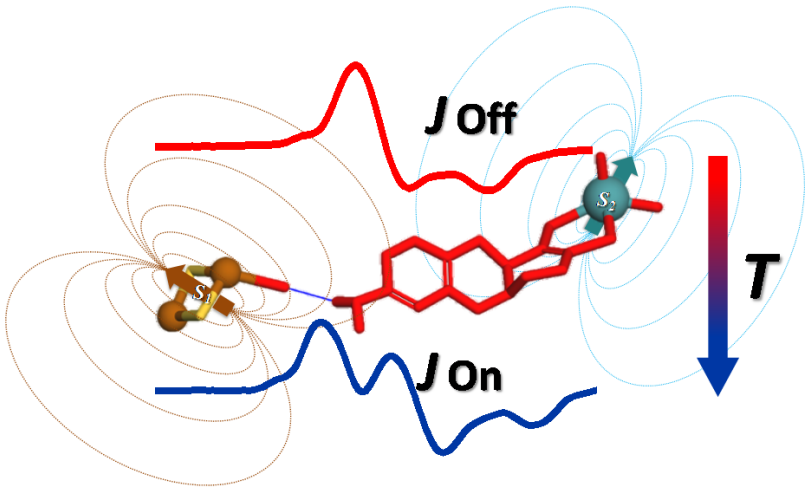

**Abstract**

Continuous Wave Electron Paramagnetic Resonance (CW EPR) is an essential spectroscopic tool to study systems containing unpaired electrons. The potential capability of the technique has exceeded its use solely by experts, and today is widely used by non-specialists. In this microreview we present selected examples together with basic theoretical aspects necessary to understand the EPR properties of isolated paramagnetic centers and assemblies of them which may be coupled by very weak isotropic exchange interactions ($< 0.1$ cm$^{-1}$) when linked by diamagnetic extended chemical pathways. The goal of the paper is to show in a unified way the information that CW EPR can provide to the understanding of the electronic structure and magnetic properties of distinct types of paramagnetic transition metal ion-containing systems of biological relevance such as low molecular weight inorganic complexes and metalloproteins.

## 1. Introduction

Continuous Wave Electron Paramagnetic Resonance (CW EPR) is a major spectroscopic tool used in chemistry, physics, and biology. The technique consists of the application of a static magnetic field **B** that splits the spin energy levels and a very weak oscillating magnetic field perpendicular to **B** with a frequency in the microwave range, which induces transitions between the spin energy levels.

EPR provides information about the interaction of the electron spin with the external magnetic field (Zeeman interaction), on the interaction between the unpaired electron spin (*S*) and the nuclear spins (*I*) associated with the paramagnetic center (hyperfine interaction), and on the interaction between different electron spins (isotropic exchange, dipole-dipole interaction, anisotropic and antisymmetric exchange). Most of these interactions are anisotropic, *i.e.* their values depend on the orientation of the molecular frame relative to the static magnetic field. The detailed analysis by EPR of all these interactions provides information about the electronic structure, molecular structure, and bonding of the paramagnetic center.

Although EPR is generally considered as a complex technique from both theoretical and experimental points of view compared to other spectroscopies, the potential capability of the technique has exceeded its use solely by experts, and today is widely used by non-specialists. There are several text books that cover all the basic aspects of the technique,[1] as well as many reviews and papers on EPR that cover applications in the distinct research areas in which the technique is applicable, including high-field and pulsed EPR.[1g, 2]

In this microreview we highlight the information that CW EPR can provide to the understanding of the electronic and magnetic properties of distinct types of transition metal ion-containing systems of biological relevance such as low molecular weight inorganic complexes and metalloproteins. A common point between these two systems is that the metal

centers, when linked by diamagnetic extended chemical pathways, may be coupled by very weak isotropic exchange interactions (< 0.1 $cm^{-1}$), which can be selectively and accurately evaluated by EPR, a fact that cannot be achieved by conventional magnetic measurements. The EPR study of exchange-coupled transition metal ion complexes is very relevant in different research fields such as molecular magnetism and bioinorganic/biological chemistry.[3] For the former, the information gained with these studies has been essential to establish the underlying molecular basis to design paramagnetic materials with predictable magnetic properties[4] and to design materials such as molecular-based and single-molecule magnets.[5] For the latter, EPR has been relevant to evaluate the magnetic properties not only of metal centers in biomimetic compounds and biological macromolecules but also to evaluate exchange coupling constants associated with chemical paths involved in electron transfer reactions.[6]

This microreview is organized in two main parts. In the first part we present general concepts on the theoretical aspects concerning specifically the interaction between centers, together with some examples that illustrate different situations that can occur when performing an EPR experiment on low molecular weight inorganic complexes. In the second part, we discuss the utility of EPR in the characterization of redox metalloenzymes with special emphasis on how EPR can be used to establish structure-function relationships. For both small inorganic complexes and metalloproteins we will analyze only systems containing Kramers ions with $S$= 1/2 or $S$ > 1/2 that can be treated as effective spins $S'$= 1/2.

## 2. The Exchange Interaction

The exchange phenomenon refers to an interaction transmitting electronic effects between two spins belonging to the same or distinct molecular entities. When this interaction is transmitted by a diamagnetic chemical path that links the spins, the phenomenon is also

called superexchange.[3a, 3b] We will use the two names indistinctly along the paper. This interaction, purely electrostatic in nature, yields singlet and triplet states separated by an energy gap $J$ ( $\hat{H}_{ex} = -J\hat{\mathbf{S}}_1 \cdot \hat{\mathbf{S}}_2$ ), which characterizes the interaction and is named isotropic exchange coupling constant. The singlet state is lowest when $J$ is negative (antiferromagnetic coupling), while the triplet is the lowest one when $J$ is positive (ferromagnetic coupling). The reader must be careful in the interpretation of sign and magnitude of $J$ as other conventions may be used for the exchange Hamiltonian ( $-2J\hat{\mathbf{S}}_1 \cdot \hat{\mathbf{S}}_2$, $2J\hat{\mathbf{S}}_1 \cdot \hat{\mathbf{S}}_2$, and $J\hat{\mathbf{S}}_1 \cdot \hat{\mathbf{S}}_2$). The magnitude of $J$ is mainly determined by factors such as the distance between centers and the nature and the structural topology of the bridging chemical path.[2b, 4a] The dependence on the distance for long bridging chemical paths was analyzed empirically by Hoffman *et al* on the basis of experimental data in simple inorganic systems showing weak exchange interactions ($|J| < 0.1$ cm$^{-1}$), who found that $J$ decreases exponentially with distance.[2b] The topological factor is also central to determine not only the magnitude of $J$ but also its sign, though for extended chemical bridging paths as the ones found in metalloproteins $J$ was always found to be antiferromagnetic.

The exchange coupling constant can be considered as the sum of two antagonistic contributions, $J = J_F + J_{AF}$, where $J_F$, the ferromagnetic contribution, tends to align the spins parallel, and $J_{AF}$, the antiferromagnetic contribution, antiparallel. The magnitude and sign of $J$ may be analyzed on the basis of a qualitative model proposed by Kahn that uses non orthogonal molecular orbitals centered on each spin of a dinuclear unit. [3a] In this model, both contributions to $J$ depend on the overlap density $\rho(i)$ in the bridging pathway, $\rho(i) = \Phi_1(i)\Phi_2(i)$, where, $\Phi_1$ and $\Phi_2$ are the magnetic orbitals (orbitals containing the unpaired electron) of atoms 1 and 2, and i identifies the unpaired electrons. $J_F$ is proportional to the electrostatic repulsion of the overlap densities of the two interacting spins, whereas $J_{AF}$ to the overlap integral. For interacting spins bridged by long chemical paths, the overlap integral

dominates over the electrostatic repulsion of the overlap densities, which explains the negative values of *J* found in most metalloproteins.

## 3. Types of Samples in EPR Spectroscopy

The usual samples employed in EPR studies in chemistry labs may be in the form of fluid and frozen solutions, powders, or single crystals. In a fluid solution, especially for low viscosity solvents, the paramagnetic species can tumble very rapidly, simplifying the EPR spectra as the molecular tumbling averages out the anisotropic interactions contributing to the spectra. In contrast, in viscous and frozen solutions molecules are hindered or not able to move, respectively, and the sample contains a random distribution of all possible molecule orientations with respect to the static magnetic field, which means that there is an equal probability for the magnetic field to have any orientation with respect to the molecular framework. This situation also occurs in powdered samples, which are constituted by lots of microcrystals randomly oriented. It is important to note that in all these samples EPR spectra are invariant to sample rotation.

When EPR is performed on oriented single crystals, the molecules in the crystal have a unique orientation with respect to the static magnetic field and therefore orientation-dependent EPR spectra can be measured. As a consequence, the information obtained from single crystal EPR experiments is much more complete than that obtained from randomly oriented samples, as this particular methodology allows one to characterize completely the anisotropic interactions. Information about single crystal mounting, single crystal EPR spectra acquisition, and data analysis can be found in the literature.[2c, 7]

## 4. Magnetically Diluted Systems

### 4.1 EPR of Mononuclear Metal Compounds

From a magnetic point of view, the term *magnetically diluted* is applicable to a system having non-interacting paramagnetic centers, a situation that occurs when the paramagnetic centers are sufficiently far removed from each other, usually at distances larger than 30 Å.[2b] Examples of magnetically diluted systems are diamagnetic hosts doped with paramagnetic impurities, diluted solutions of metal complexes, and metalloproteins. The field-dependent energies of the spin states of a magnetically diluted system containing a mononuclear $S$= 1/2 metal center are determined by the eigenvalues of the spin Hamiltonian

$$\hat{H} = \mu_B \mathbf{B}\cdot\mathbf{g}\cdot\hat{\mathbf{S}} + \hat{\mathbf{I}}\cdot\mathbf{A}\cdot\hat{\mathbf{S}} \qquad (1)$$

where the first and second terms are the Zeeman and hyperfine interactions, respectively, $\mu_B$ is the Bohr magneton, **B** is the static magnetic field, $\hat{\mathbf{S}}$ and $\hat{\mathbf{I}}$ are the electron and nuclear spin operators, respectively, and **g** and **A** are 3×3 matrices. Equation (1) only includes the hyperfine interaction between the electron spin and the nuclear spin of its own nucleus for simplicity. Also, the nuclear Zeeman and quadrupolar interactions are omitted as, with a few exceptions, they are not usually detected in CW EPR.[8]

EPR spectra of polycrystalline solids or frozen solutions of mononuclear metal centers are classified according to the **g**-matrix symmetry in rhombic, axial, and isotropic. The **g**-matrix in rhombic spectra, which is the most general case, is characterized by three distinct $g$-factors ($g_x, g_y, g_z$) called the eigenvalues or principal values of the **g**-matrix (Figure 1). The indexes x,y,z correspond to specific directions in the molecular frame called the eigenvectors or principal directions in which the **g**-matrix is diagonal. There is no convention to assign a specific eigenvalue to any index, and the nomenclature x,y,z or 1,2,3 will be used indistinctly along the paper. Axially symmetric spectra are associated with a **g**-matrix with two equal eigenvalues ($g_x = g_y = g_\perp \neq g_z = g_\parallel$), whereas for isotropic spectra $g_x = g_y = g_z = g_{iso}$ (Figure 1).

The *g*-values can be simply used as a fingerprint of the complex, or, ideally, should be utilized to study geometric structure, bonding, and electronic structure of the paramagnetic center. Particularly, the geometric structural information that can be obtained from the **g**-matrix evaluation in magnetically diluted compounds is related to the symmetry of the metal site, as the symmetry of the **g**- and **A**-matrices must be compatible with the coordination geometry of the paramagnetic center.

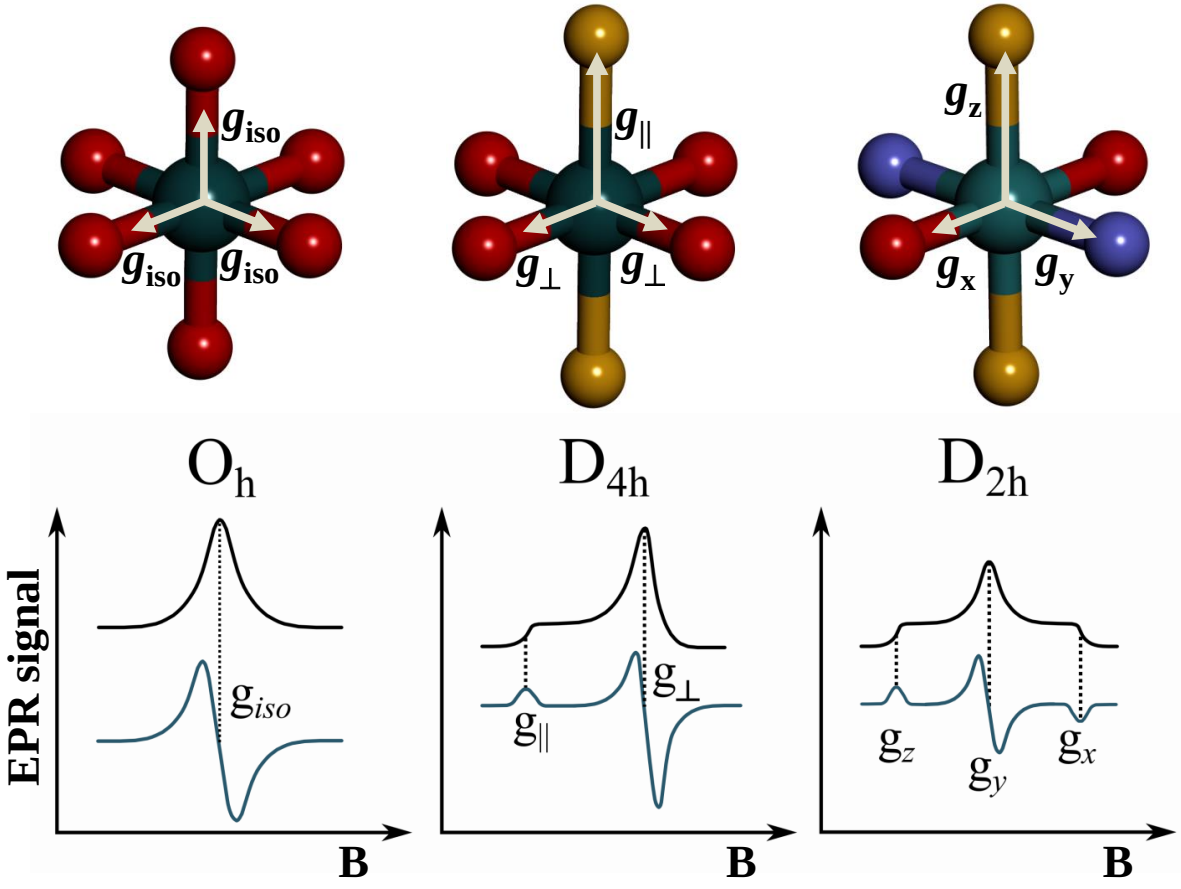


Figure 1. **g**-matrix symmetry and associated absorption (black) and first-derivative (dark cyan) EPR spectra for three coordination geometries: octahedral ($O_h$) (left), octahedral with tetragonal distortion ($D_{4h}$) (center) and orthorhombic ($D_{2h}$) (right). The different colors represent different atoms and/or different bond-distances. The examples correspond to the cases $g_{\parallel} > g_{\perp}$ and $g_z > g_y > g_x$.

As shown in Figure 1, for metal sites with strict axial symmetry (*e.g.* molecules belonging to point group $D_{4h}$), the eigenvector associated with $g_{\parallel}$ must lie on the axial axis (the unique molecular z axis), whereas the remaining two eigenvectors associated with the two $g_{\perp}$ eigenvalues must lie on the equatorial ligand plane. For metal sites with lower symmetry but still presenting an axial distortion, *e.g.* $D_{2h}$, the $g_{x,y}$ eigenvectors must lie also on the equatorial ligand plane but pointing either along the bonds or between the bonds. Departures from these idealized geometries are found in most paramagnetic systems, which are reflected with different extents in their EPR properties. However, when this departure is not considerable, the **g**-matrix may follow the approximate symmetry around the metal site, which results in nearly axial **g**-matrices with eigenvectors lying approximately along molecular directions close to the true axes in an idealized symmetry. These particular molecular directions are usually identified as molecular pseudo symmetry axes. Systems with these characteristics were reported for copper(II) and molybdenum(V) complexes in nearly square planar coordination. [7b, 9] The assumption that eigenvectors lie along molecular pseudo symmetry axes may not be true for systems with spins higher than 1/2 which are usually analyzed as effective spins $S' = 1/2$, as is the case of high-spin Co(II) ($S = 3/2$). Except for those cases with strict symmetry,[10] a small departure from the idealized symmetry in high spin Co(II) compounds having large **g**-anisotropy can occasion drastic changes in the **g**-matrix orientation.[11] The above symmetry considerations may be utilized to propose the eigenvectors of **g**-matrices when this information is unknown.

Additional information on structure, bonding, and electronic properties of the metal site can be obtained from the analysis of the hyperfine coupling interaction with its own nucleus and of that with the ligand nuclei, which is also called superhyperfine interaction. This analysis is useful to study the chemical composition of the metal center, and can also provide information about its coordination geometry and chemical bonding. However, one should have in mind that hyperfine couplings, particularly those with metal ligands, are in some cases too small to be resolved by conventional CW EPR techniques, in which case EPR-based techniques such as electron nuclear double resonance (ENDOR) may recover the information hidden in the linewidth in the EPR spectra.[12] It is important to note that when the hyperfine structure is resolved in the EPR experiment, the information provided by both techniques is identical.

There are some useful correlations in EPR spectroscopy that allow one to learn about the structure and bonding of metal complexes. One of these correlations was proposed by Peisach and Blumberg who plot $A_{\|}$ *vs* $g_{\|}$ values for copper metal complexes showing nearly axially symmetric EPR signals.[13] One of the advantages of this correlation is that one obtains with a certain confidence the number and type of copper equatorial ligands. A weakness of the correlation is that it does not take into consideration the type of axial ligands. Another example of magneto-structural correlations were proposed for V(IV) and Cr(V) complexes. The former, which is called additivity relationship, was proposed by Wuthrich [14] and later refined by Chasteen, [15] which allows the hyperfine coupling constant, specifically $A_{\|}$, to be correlated to the number and types of ligands present in the equatorial plane of V(IV) complexes. The latter, which was proposed by Barr-David et al, is an empirical method

developed for determining the coordination number of Cr(V) complexes (five- or six-coordinate) and the donor groups bound to Cr(V) from the measured $g_{iso}$ and $A_{iso}$ values.[16]

### 4.2. Dinuclear Metal Compounds

The simplest dinuclear unit is formed by two interacting paramagnetic ions with $S$= 1/2 spins, which are commonly found in several inorganic complexes as well as in metalloproteins.[3d, 4a, 17] The EPR behavior of these dinuclear units may be considerably different of that corresponding to the mononuclear centers, because the isotropic exchange interaction couples the spins to give singlet ($S$= 0) and triplet ($S$= 1) states (section 2).[1a, 3a] The spin Hamiltonian describing the energy levels of a dimer composed of two dissimilar $S$= 1/2 spins is given by

$$\hat{\mathrm{H}} = \mu_B \hat{\mathbf{S}}_1 \cdot \mathbf{g}_1 \cdot \mathbf{B} + \mu_B \hat{\mathbf{S}}_2 \cdot \mathbf{g}_2 \cdot \mathbf{B} + \hat{\mathbf{S}}_1 \cdot \mathrm{A}_1 \cdot \hat{\mathrm{I}}_1 + \hat{\mathbf{S}}_2 \cdot \mathrm{A}_2 \cdot \hat{\mathrm{I}}_2 + \hat{\mathbf{S}}_1 \cdot \mathrm{J} \cdot \hat{\mathbf{S}}_2 \qquad (2)$$

where the last term takes into account the interaction between the two spins, which is characterized by the **J**-matrix. Equation (2) only includes the hyperfine interaction between the electron spin on each center and the nuclear spin of its own nucleus (cross hyperfine terms are not considered). The interaction term $\hat{\mathbf{S}}_1 \cdot \mathbf{J} \cdot \hat{\mathbf{S}}_2$ in Equation (2) can alternatively be written as

$$\hat{\mathbf{S}}_1 \cdot \mathbf{J} \cdot \hat{\mathbf{S}}_2 = -J\hat{\mathbf{S}}_1 \cdot \hat{\mathbf{S}}_2 + \hat{\mathbf{S}}_1 \cdot \mathbf{D} \cdot \hat{\mathbf{S}}_2 + \mathbf{d} \cdot \hat{\mathbf{S}}_1 \times \hat{\mathbf{S}}_2 \qquad (3)$$

where the first term is the isotropic exchange, the second one corresponds to the sum of anisotropic exchange and dipole-dipole interactions, and the third term is the antisymmetric exchange. The origin and the effect of each term on the spin system have been extensively described elsewhere.[1a, 3b, 18] We will briefly describe the cases in which the isotropic exchange interaction is larger than all the other terms in Equation (2) (strong exchange limit) and in which $J$ is small (weak exchange limit), with special emphasis in the latter as it will be used to understand structural and functional aspect of metalloenzymes.

For $J >> h\nu$ (strong exchange limit), where $h\nu$ is the energy of the microwave radiation, the isotropic exchange interaction splits the singlet and triplet states of the dimer by an energy amount $J$, whereas the remaining interactions cause the three-fold degeneracy of the triplet state to be removed even in zero magnetic field (ZFS). The energy levels of the spin Hamiltonian for an $S$= 1 state arising from two similar $S$= 1/2 ions can be written ignoring the singlet state as

$$\hat{H} = \mu_B \hat{\mathbf{S}} \cdot \mathbf{g} \cdot \mathbf{B} + \hat{\mathbf{S}} \cdot \mathbf{A} / 2 \cdot \hat{\mathbf{I}}_1 + \hat{\mathbf{S}} \cdot \mathbf{A} / 2 \cdot \hat{\mathbf{I}}_2 + \hat{\mathbf{S}} \cdot \mathbf{D} \cdot \hat{\mathbf{S}} \qquad (4)$$

where $\hat{\mathbf{S}} = \hat{\mathbf{S}}_1 + \hat{\mathbf{S}}_2$, $\mathbf{g}$= $\mathbf{g}_1$= $\mathbf{g}_2$, and $\mathbf{D}$ is half of that defined in Equation (3). Note that antisymmetric exchange is omitted because this interaction is zero when the individual sites show identical $\mathbf{g}$ matrices. In the $\mathbf{D}$-matrix principal axes frame ($X$,$Y$,$Z$) the term $\hat{\mathbf{S}} \cdot \mathbf{D} \cdot \hat{\mathbf{S}}$ can alternatively be written as $D(\hat{S}_Z^2 - \frac{1}{3}\hat{S}^2) + E(\hat{S}_X^2 - \hat{S}_Y^2)$, where $D$ and $E$ are scalar magnitudes related to the eigenvalues of the $\mathbf{D}$-matrix by $D = \frac{3}{2} D_Z$ and $E = \frac{1}{2}(D_X - D_Y)$. For dinuclear units formed by spins $S_1$ and $S_2$ different from 1/2, the states of the pair are classified according to the angular moment addition rules, with the ground state being $|S_1 - S_2|$ for an antiferromagnetic interaction or $|S_1 + S_2|$ for a ferromagnetic interaction.

Figure 2 schematizes the effect of $J$ and $\mathbf{D}$ on the energy levels of a strongly coupled dimer composed of two similar $S$= 1/2 spins with $D < 0$ and $E$= 0.

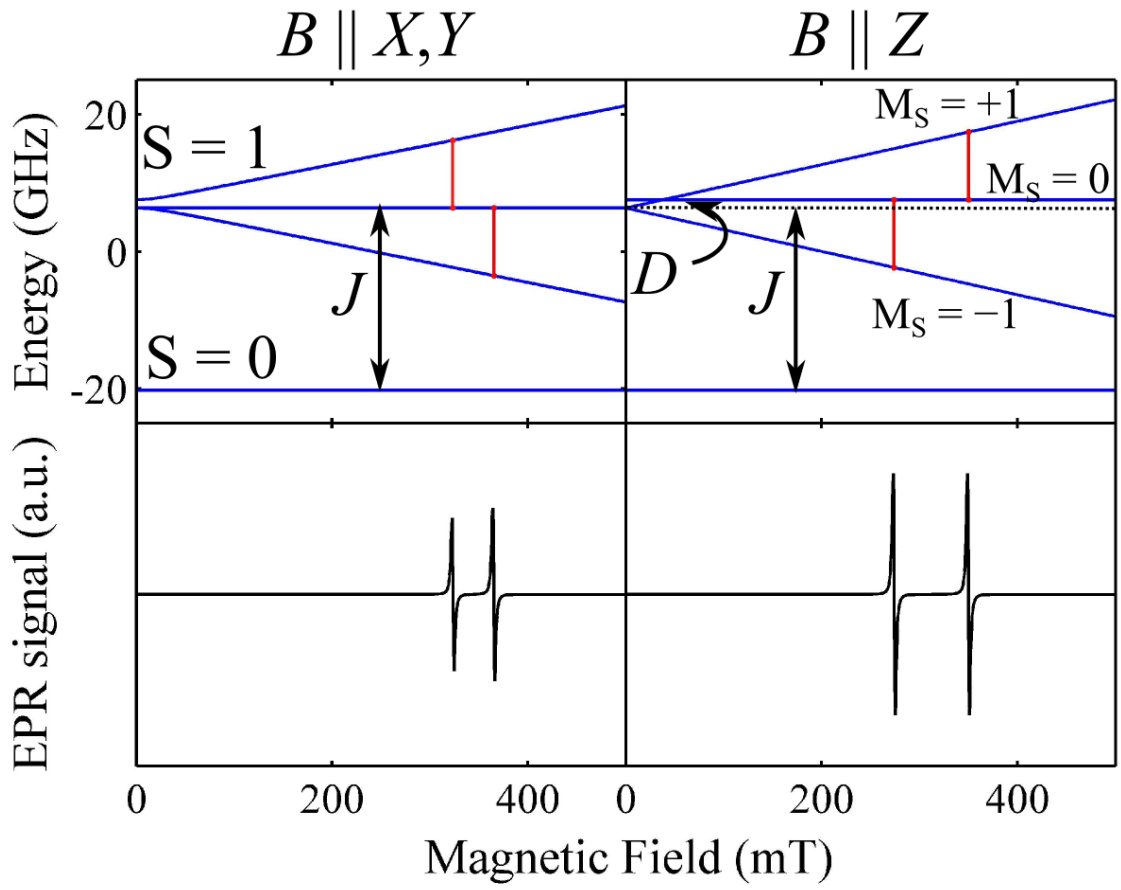


Figure 2. Spin system energies and resonances obtained from numerical diagonalization of Equation (2) as a function of applied magnetic field of a strong exchange coupled dimer of similar $S$= 1/2 spins for $J$ < 0 (antiferromagnetic), $D$ < 0, and $E$= 0. Hyperfine interactions are ignored. The red lines are allowed transitions ($\Delta M_S = \pm 1$). $X$,$Y$, and $Z$ correspond to the principal directions of **D**. Simulation parameters were $J$= -0.9 cm$^{-1}$, $D$= -0.04 cm$^{-1}$ and $\nu$= 9.87 GHz. The dotted line in the right panel corresponds to the $M_S$= 0 energy level for $D$= 0.

As shown in this figure, spectra for a given magnetic field orientation show two resonance lines centered at $g = h\nu/\mu_B B$, which can give rise to different types of spectra in powder and powder-like samples depending on the strength of the ZFS. Dimer EPR spectra are dependent on temperature, as the singlet and triplet populations vary with temperature. For the case of the antiferromagnetically coupled dimer shown in Figure 2, the lower the temperature the

lower the population of the triplet state, determining that at $kT << J$ , no EPR signal can be detected. Examples of dimer EPR spectra in the strong exchange limit with different ZFS values are widely described in the literature.[19]

For $J < h\nu$ (weak exchange limit) and $\mathbf{g}_1 \neq \mathbf{g}_2$, anisotropic interactions mix appreciably the singlet and triplet states, which therefore cannot be considered pure. This situation, observable normally for distant metal centers connected by long chemical paths in metalloproteins, leads to very different EPR spectra to those obtained for $J >> h\nu$. Figure 3 shows the spin energies obtained from numerical diagonalization of Equation (2) as a function of the static magnetic field along the interspin direction of a very weak exchange coupled dimer of dissimilar $S$= 1/2 spins for $J < 0$. Equation (2) predicts in the absence of both hyperfine and spin-spin interactions two resonance lines separated by $\Delta B = h\nu\Delta g/\mu_B g_1 g_2$, in which $\Delta g = |g_1 - g_2|$. Note that $\Delta B$ depends on the orientation of the static magnetic field relative to the molecular frame, and its value depends on the magnitude of $J$ and all the other anisotropic spin-spin interactions defined above (Equation (3)). It has been adopted that when $J < 30$ cm$^{-1}$ , the anisotropic exchange may be neglected which determines that **D** can be assumed to be determined by the dipole-dipole interaction.[20] We will assume in all the cases we analyze that both anisotropic and antisymmetric exchange are negligible, and hence the splitting of the resonance lines are determined solely by isotropic and dipole-dipole interaction. Hence, when $J+D_{dip}$, where $D_{dip}$ is the value of **D** for a given angle between the interspin direction and the static magnetic field, is different from zero and much lower than $\Delta B$ , these lines are each split into doublets with a splitting equal to $J+D_{dip}$ (upper panel in Figure 3). Furthermore, the split lines have approximately the same intensity (lower panel in Figure 3). When $J+D_{dip}$ is comparable with $\Delta B$ but still lower, two doublets with splitting $J+D_{dip}$ are also obtained but with the outer lines being less intense than the two central ones.

Two lines with the same intensity separated by $D_{dip}$ are observed when $J+D_{dip} > \Delta B$. If in addition, hyperfine interactions are present, more complicated EPR spectra may be obtained (not shown). The analysis of the nature of magnetic coupling between two centers as well as the determination of $J$ using Equation (2) are relevant as they allow one to learn about structural properties and electron transfer processes occurring in redox metalloenzymes (sections 6.4 and 6.7).

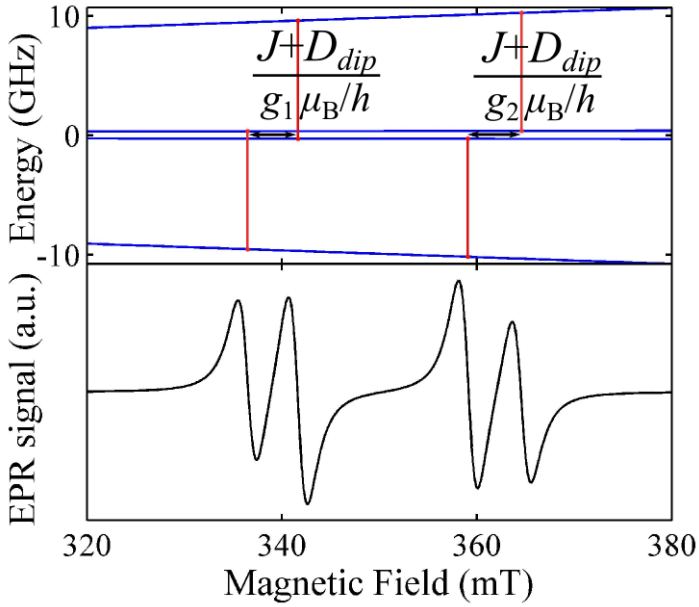


Figure 3. Spin system energies obtained with Equation (2) as a function of applied magnetic field along the interspin direction of a very weak exchange coupled dimer of dissimilar $S$= 1/2 spins for $J$ < 0 (upper) together with the corresponding EPR spectra (lower). Hyperfine interactions are ignored. The allowed transitions are indicated with red lines. The splitting $J+D_{dip}$ in magnetic field units are also indicated. EPR parameters were $g_1$= 1.95, $g_2$= 2.08, $J$= -100 MHz and $D_{dip}$= -50 MHz.

### 4.3 EPR simulation of solution and powder samples and applications

The accurate determination of EPR parameters from powder samples, frozen, and fluid solutions requires normally spectral simulation. These routine EPR simulations aim to obtain the values of the relevant parameters that determine the energy of the system, *i.e.* **g** and **A** matrices for a system described by Equation (1). There are several programs to perform EPR simulations such as XSophe®,[21] Spinach,[22] and Easyspin.[23] The information that can be obtained depends on the type of sample. Whereas spectral analysis of frozen solutions and powder samples of a magnetically diluted mononuclear system may yield the eigenvalues of **g** and **A** matrices, usually only their isotropic average ($g_{iso}$, and $A_{iso}$) may be obtained from a fluid solution, this being possible only when the molecule tumbling is fast enough to average out all the anisotropies. The information obtained from these types of samples is limited only to the eigenvalues, as the eigenvectors of both **g** and **A** cannot be determined, although in some cases the relative orientation between some of the eigenvectors associated with both matrices can be determined to some accuracy. This analysis is also applicable to magnetically diluted dinuclear units. However, note that the isotropic exchange coupling constants *J* can be evaluated only for dinuclear units in the weak exchange limit (Figure 3), as for the strong exchange limit, exchange interaction contributes only a common constant to the triplet energy levels.

An important branch of bioinorganic chemistry is devoted to study paramagnetic metal complexes that serve as biocatalysts in solution. [24] Although the biological function of these compounds is carried out in solution, their structure is normally determined in the solid state. A common question that can be solved by EPR is whether the structure of the solid state compound corresponds to that in solution or not. Figure 4, lower panel, shows water solution and powder EPR spectra of the complex Cu(II)(L-glutamate)$(H_2O)_2$ (Cuglu) and its Cu(II)-

doped isostructural Zn(II) analogue (CuZnglu), which present a 2D polymeric structure in the solid state (Figure 4, upper panel).[25] Spectra a and b show typical Cu(II) ion EPR spectra showing hyperfine interaction with the copper nucleus ($I$= 3/2). The room temperature solution spectrum (spectrum a) is what is called a slow-motion EPR spectrum in which the anisotropic parameters $g$ and $A$ are partially averaged due to molecular tumbling.[26] This spectrum shows two overlapped components, one more important with $g_{iso}$= 2.158, $A_{iso}$= 57 × $10^{-4}$ $cm^{-1}$) and a second less intense one corresponding to a Cu(II) species that shows only the EPR $m_I$= -3/2 feature discernible. Figure 4, spectrum b, shows the powder EPR spectrum of CuZnglu, where substitutional Cu(II) ions are magnetically isolated. Simulation of this spectrum yielded the **g** and **A** matrix parameters given in the caption to Figure 4, from which one can obtain $g_{iso} = (g_1 + g_2 + g_3)/3 = 2.163$, $A_{iso} = (A_1 + A_2 + A_3)/3 = 54 \times 10^{-4}$ $cm^{-1}$, in a good agreement with the $g$- and $A$-values from fluid solution. Thus, it can be concluded that the coordination environment of the copper in the solid state structure is kept in solution, though a small fraction adopts a different conformation. The spectrum of the pure compound (Figure 4, spectrum c), which looks very different to the others, is included to show that the EPR parameters obtained by simulation (see caption to the figure), although related with, are not equal to those of individual Cu(II) centers, a phenomenon related to the interaction between metal centers in an extended lattice, which will be discussed below. This example clearly illustrates that the information provided by EPR from a magnetically undiluted compound does not necessarily reflect the molecular properties of the individual paramagnetic center.

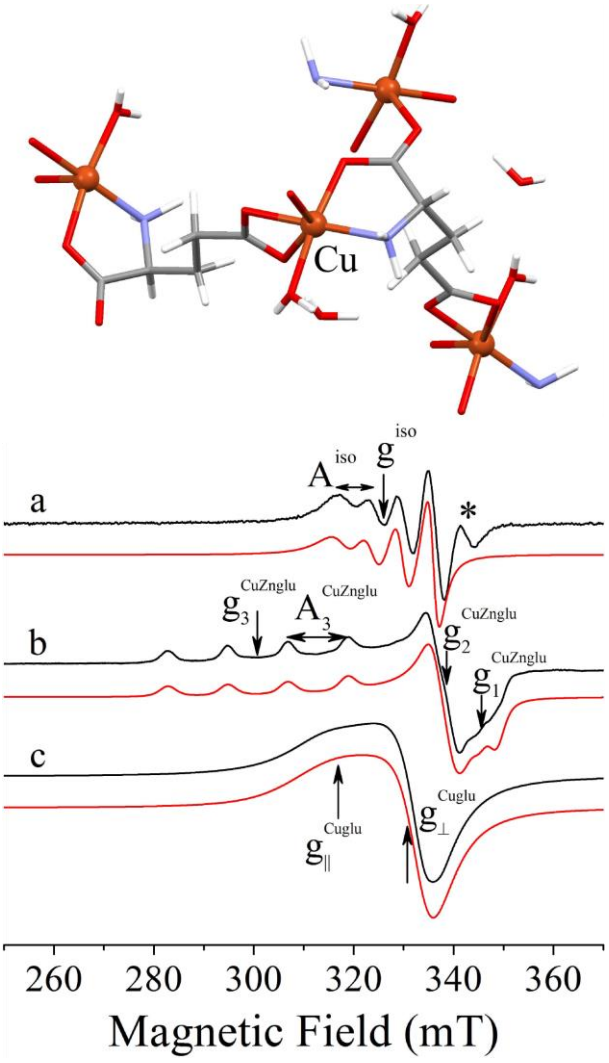


Figure 4. Upper. Structure of Cu(II)(L-glutamate)$(H_2O)_2$ (Cuglu). Lower. X-band EPR spectra (~ 9.8 GHz) obtained on a) Cuglu water solution at room temperature, b) CuZnglu microcrystalline powder, c) pure Cuglu microcrystalline powder. Spectrum a shows an additional peak marked with an asterisk due to a secondary species formed in solution. EPR parameters obtained by simulation (red lines) were a) $g_{iso}$= 2.158, $A_{iso}$= 57 × $10^{-4}$ $cm^{-1}$; b) $g_{1,2,3}$= 2.050, 2.093, 2.345, $A_{1,2,3}$= 37 × $10^{-4}$ $cm^{-1}$, n.d., 124 × $10^{-4}$ $cm^{-1}$; c) $g_{\perp}$= 2.115, $g_{||}$= 2.240. n.d., non-detectable.

## 5. Magnetically Undiluted Systems: Dynamical Effects Produced by Intercenter Isotropic Exchange Interaction

The EPR spectra of pure paramagnetic compounds, i.e. systems in which the paramagnetic centers are not diluted, are dominated by the interaction between the centers and therefore yield little information about the individual centers (Figure 4). These intercenter interactions are the same as the ones defined above for a dinuclear unit (isotropic, antisymmetric, and anisotropic exchange and dipolar interaction), but summed over all paramagnetic neighbors in an infinite lattice.[25] Particularly, intercenter isotropic exchange interaction in an extended compound produces dynamical effects on the spin system, and its more notorious effect on the spectra is to merge the resonance lines associated with the isolated centers, in contrast with all the other interactions that produce line broadening. The problem of extended interactions in 1D, 2D, and 3D lattices has been extensively studied because of their physical significance, and the knowledge acquired was employed to characterize extended compounds with metal centers coupled by superexchange. The relevance of these investigations is wide, since they impact on very different research fields such as molecular magnetism, spintronics, and electron transfer processes in systems of biological interest.[4b, 27]

The changes experienced by the EPR spectra of extended lattices of paramagnetic centers coupled by intercenter isotropic exchange interaction can be rationalized using the "random frequency modulation model" introduced by Anderson.[26, 28] Figure 5 schematizes the changes experienced in the EPR spectra due to the exchange phenomenon for a system having two dissimilar $S$= 1/2 spins without hyperfine interaction. In the absence of exchange interaction ($J$= 0), the spectrum consists of two resonance lines at positions $B_1$ and $B_2$, each with equal transition probabilities, separated $\Delta B = |B_1 - B_2|$. In the presence of exchange, the spins giving rise to these two lines jump back and forth in a random way with an exchange

frequency of the order of $J$. The model predicts different kinds of spectra depending on the ratio between $J$ and $\Delta B$. For $J < \Delta B/2$ (weak exchange regime), the two resonance lines at positions $B_1$ and $B_2$ are broadened by exchange and shifted towards the gravity center of the spectrum; the larger the $J$ the larger the shift. For $J > \Delta B/2$ (strong exchange regime), a unique exchange collapsed Lorentzian-shaped resonance line is obtained, with exchange yielding narrowing rather than broadening (linewidth proportional to $1/J$). A unique broad central resonance line with is obtained for $J \approx \Delta B/2$.

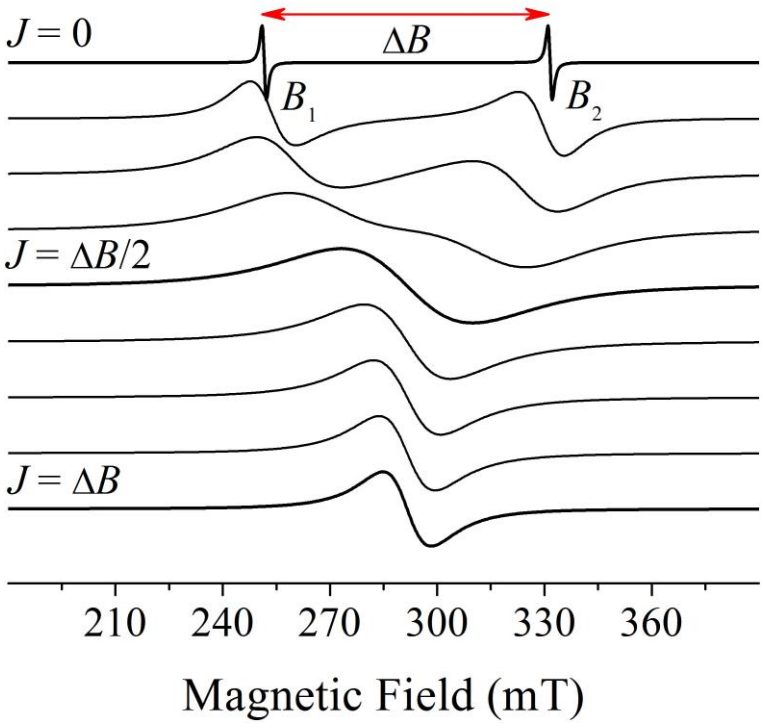


Figure 5. Computed X-band EPR spectra predicted by the "random frequency modulation model" for an extended system having two dissimilar $S$= 1/2 spins with no hyperfine interaction for different ratios between $J$ and $\Delta B$.

Analytical solutions of the exchange narrowing phenomenon based on Anderson´s theory exist for the simplest cases of systems showing two-line spectra arising from extended lattices containing two dissimilar spins, a single spin coupled by hyperfine interaction with a

nuclear spin $I$= 1/2, and interacting $S$= 1 dimers,[29] which can alternatively be obtained from generalized Bloch equation.[2b] As the number of resonances increases, the analytical solutions first become impractical and soon impossible, and a numerical solution is needed. The relevance of Anderson´s model is that it explains all the different exchange regimes depicted in Figure 5 using a unique equation.[11a, 30]

There are many examples in the literature describing the magnetic properties of spins coupled by exchange in extended compounds. We have selected an EPR study performed on a mononuclear Co(II) compound to illustrate the effect of isotropic exchange on the resonance lines corresponding to isolated Co(II) centers. Figure 6 shows EPR spectra of the coordination polymer *catena*-(*trans*-($\mu$2-fumarato)tetraaquacobalt(II)) and its Co(II)-doped isostructural Zn(II) analogue, where the Co(II) ions are in a high spin configuration that can be treated as an effective spin $S´$= 1/2. [11a] The metal centers in this Co(II) ion complex are linked by two different types of superexchange paths, one involving a fumarate dianion ($J_{AA}$) and the other a triple hydrogen bond ($J_{AB}$). This 3D extended lattice is composed of two chemically identical but rotated cobalt sites, identified as $Co_A$ and $Co_B$ in Figure 6 (left top panel), and hence magnetically inequivalent. The powder EPR spectrum of the diamagnetic host doped with the lowest Co(II) concentration (Co:Zn ratio of 1:30) is nearly axial with $g_\perp > g_\parallel$ and shows resolved hyperfine structure with the cobalt nucleus ($I$= 7/2). Increasing Co(II) ion doping concentration in the diamagnetic host broadens the resonance lines, making the hyperfine structure less resolved, a phenomenon due to through-space intercenter magnetic interactions that produces broadening rather than narrowing, but does not produce significant shift of the $g_\perp$ and $g_\parallel$ features. A rather distinct situation is observed in the pure compound, in which exchange interaction yields a single broad EPR resonance line. The information that can be obtained from the EPR powder spectrum of the pure compound is very limited, as one can only conclude that the Co(II) ions are in a high spin configuration and that the Co(II) ions are

likely coupled by exchange. In contrast, the information obtained from single crystal EPR spectroscopy of both doped and pure compounds (Figure 6, left bottom panel) is richer, as the full analyses of the spectral angular variation performed on the diluted compound allows one to obtain the full **g** and **A** matrices. This information, when complemented with that obtained from the pure compound, is used to evaluate selectively and accurately the two exchange coupling constants ($J_{AA}$ and $J_{AB}$) associated with the two different types of chemical pathways connecting the Co sites.[11a] In summary, this example shows very clearly the effect produced by isotropic exchange on the EPR spectra associated with isolated Co(II) ions and illustrate the potential of EPR to evaluate very weak exchange coupling constants in extended compounds using Anderson´s theory. Other examples concerning the collapse of the fine structure in a dinuclear unit and of the hyperfine structure in a mononuclear compound can be found in the literature.[30-31]

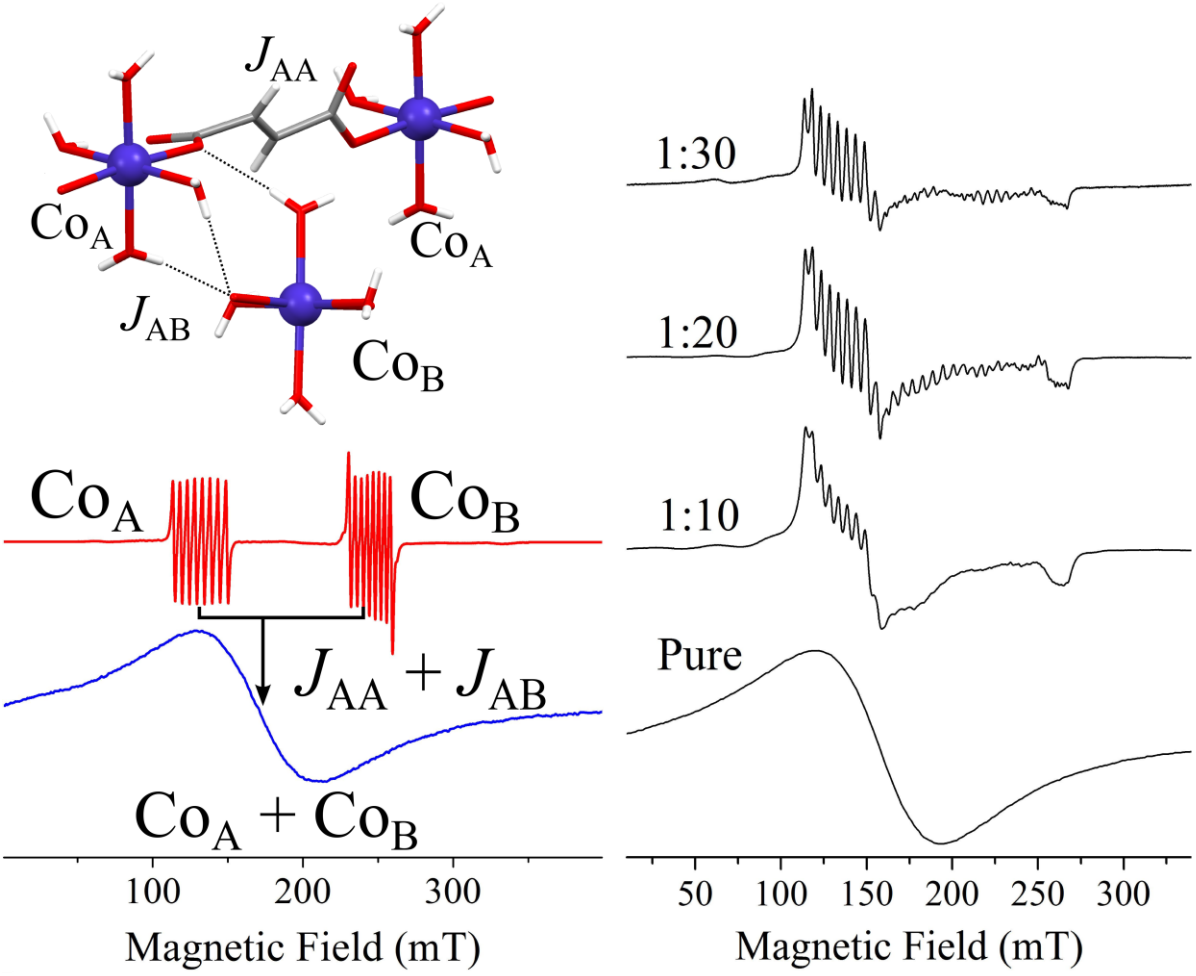


Figure 6. Structure of the coordination polymer *catena*-(*trans*-(*μ*2-fumarato)tetraaquacobalt(II)) (left top) showing the superexchange chemical paths;[32] single crystal EPR spectra for nearly the same magnetic field orientation in the Co-(II)-doped Zn(II) analogue (red), showing the resolved octets from magnetically non-equivalent sites, and in the pure Co(II) compound (blue), showing a single collapsed resonance at the spectral gravity center (left bottom); powder EPR spectra for different Co(II):Zn(II) ratios in Co(II)-doped Zn(II) compound and in the pure compound showing the collapse of the hyperfine structure and main *g*-features of individual Co(II) sites (right).

**6. CW EPR of Biological Macromolecules**

About a third of all proteins present in living organisms contain one or more redox active transition metal ions as prosthetic groups.[33] In general these proteins are metalloenzymes that catalyze specific reactions in which the metal ions form part either of the enzyme active site or function as electron transfer centers. A large group of metalloenzymes are oxidoreductases that catalyze a wide spectrum of redox reactions that occur in nature. These enzymes incorporate 81 % of the total Fe found in living organisms, as well as 93% of the total Cu, and 81% of total Mo plus W.[34] These four metals are the so-called redox-active elements of life since they can exist in several oxidation states within the physiological range of electrochemical potential (*ca* from -700 to +800 mV, *vs* NHE). The redox cycling of these transition metal ions makes it possible that they can act as electron conduits routing electrons from the enzyme active site to the redox partner and *vice versa*. As the metal centers in metalloproteins may be paramagnetic in certain oxidation states, EPR becomes a powerful technique in their characterization. Specifically, we will show how the technique can be used to detect changes in oxidation states of the metal centers, the binding of substrate and exogenous ligands to the enzyme active sites, to solve structural aspects that cannot be determined by conventional structural techniques, and to study the factors that govern electron transfer reactions during catalysis. All these technical capabilities will be shown on the basis of two representative examples of oxidoreductases, the copper-containing nitrite reductase (Nir) and the molybdenum-containing aldehyde oxidoreductase (Aor).

### 6.1 General Structural and Mechanistic Aspects of Oxidoreductases

A brief structural description and mechanistic aspects of both Nir and Aor are given first to understand the type of information that can be obtained from EPR. Aor and Nir are distinct in both structure and function, but follow a general reaction mechanism depicted in

Figure 7, which is also followed by most oxidoreductases having a redox-active metal ion at the active site.[35]

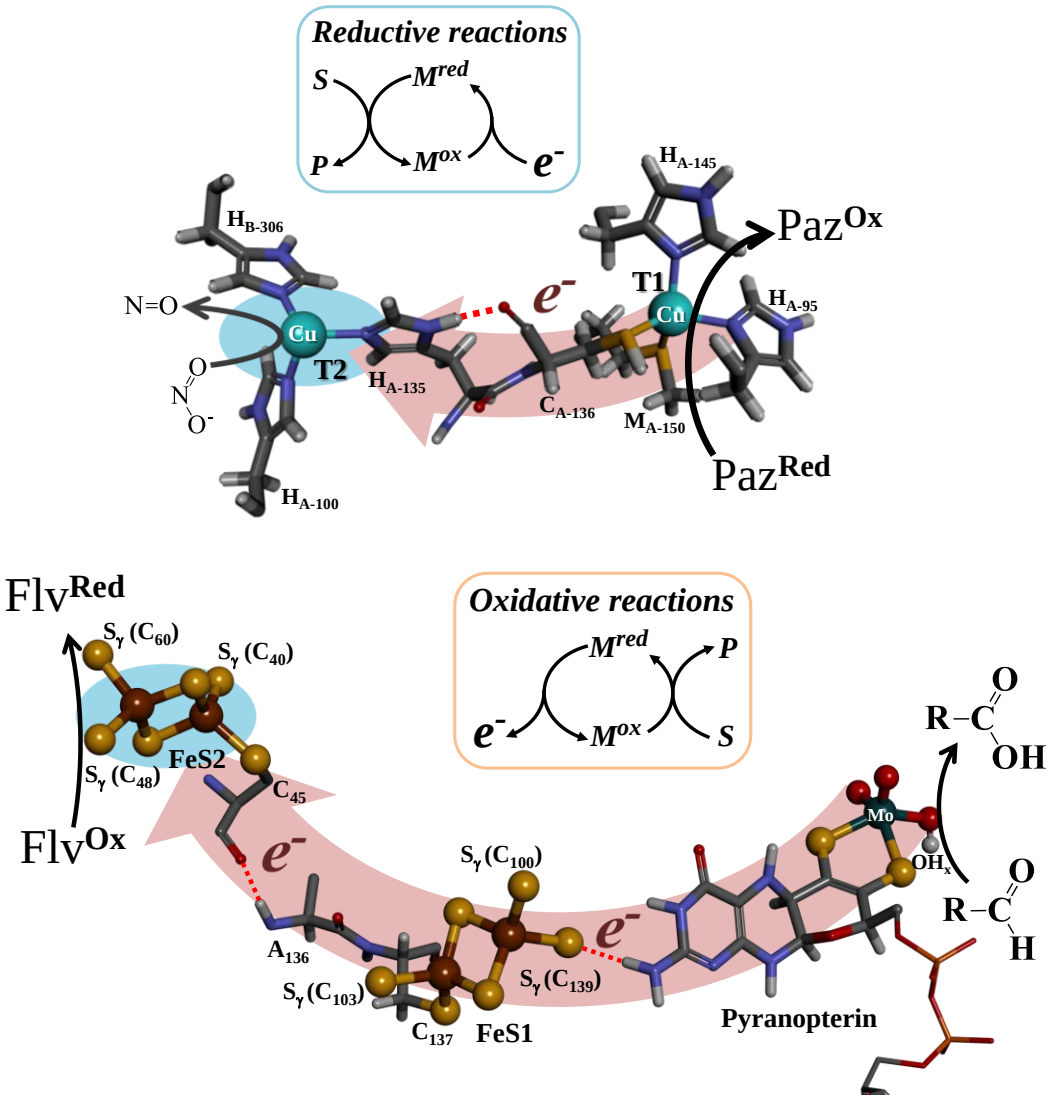


Figure 7. Enzyme reaction mechanism of Nir (top) and Aor (bottom). Pseudoazurin (Paz) and flavodoxin (Flv) are the physiological electron donor and acceptor of Nir and Aor, respectively. The $OH_x$ ligand in Aor is the catalytic labile site, which is the O-atom that reacts with the substrate. Schemes for general reductive (top) and oxidative (bottom) reactions catalyzed by oxidoreductases containing a transition metal ion in a mononuclear form at the active site are also shown. S and P stand for substrate and product, respectively. M is the

metal ion at the active site which receives/gives electrons through an electron transfer reaction mediated by the intraprotein chemical pathway. The arrows indicate the electron flow direction through the intraprotein chemical pathways. Numbering corresponds to PDB structures 1SNR and 1VLB for Nir and Aor, respectively.

As shown in Figure 7, the substrate reacts at the active site with the metal ion (M), which is reduced in those reactions that involve substrate oxidation, and oxidized in those reactions occurring in the opposite direction. The electrons generated in the course of oxidative reactions are then transferred to an external electron acceptor by means of an electron transfer process mediated by other redox cofactors present in the structure of these proteins, a copper center in Nir (T1) and iron-sulfur clusters in Aor (FeS1 and FeS2). In contrast, in reductive reactions the electron flow occurs in the opposite direction and the electrons given by an external electron donor are used to reduce the substrate.

The active site of Nir is a type 2 copper center (T2, also normal copper)[36] whereas the electron transfer copper center is of type 1 (T1, also blue copper).[36c, 37] T1 and T2 are ~12 Å apart bridged by a histidine-cysteine pathway. The proposed reaction mechanism implies that nitrite binds to T2 and is converted to nitric oxide ($NO^{\cdot}$) by one reducing equivalent delivered by T1 through the bridging chemical path. The external electron donor was identified to be a pseudoazurin, azurin or cytochrome *c*, depending on the microrganism.[35b]

Aor is an oxidoreductase with a structure more complex than Nir as it contains different types of metal ions at the active site and electron transfer centers. The active site in the as-purified form is formed by a Mo(VI) ion coordinated to two oxo, one hydroxo ($OH_x$) and two sulfur ligands provided from a dithiolene moiety which is part of a pyranopterin cytidine dinucleotide (Figure 7 bottom). This molecule, together with two iron-sulfur clusters of the type [2Fe-2S], form part of the electron transfer pathway. [38] One of the FeS clusters

(FeS1 or proximal center) is closer to the Mo site ($d_{Mo\text{-}FeS1}$= 16.2 Å) and is buried inside the protein in a domain inaccessible to solvent. The second FeS cluster (FeS2 or distal center) is situated further away from the Mo site ($d_{Mo\text{-}FeS2}$= 25.6 Å) near the protein surface and it mediates the electron transfer from Aor to the physiological electron acceptor (Flv).[39] The aldehyde oxidation catalyzed by Aor occurs at the Mo center which is, after interaction with substrate, reduced from Mo(VI) to Mo(IV). The two reducing equivalents generated in the course of the reaction are then transferred to an external electron acceptor (Flv) through the electron transfer pathway shown in Figure 7.

### 6.2 General Aspects on the CW EPR Characterization of Metal Centers in Metalloenzymes

Due to the large size of the molecule, metalloproteins in solution and crystalline forms can be considered as magnetically diluted systems. However, a different picture may emerge inside the protein molecule in those systems containing at least two paramagnetic centers, as very weak intercenter magnetic interactions may modify the EPR spectra of the individual centers. The EPR characterization of redox proteins is usually performed in the electrochemical potential range -700 to 800 mV *vs* NHE as, as stated above, most redox couples relevant in biology fall in this range. The purpose of this characterization is not only to obtain an EPR signal as a fingerprint of the metal centers, but also to estimate their reduction potentials, as well as to detect the presence of weak intercenter magnetic interactions.

Figure 8A shows the EPR spectra of as-purified Nir (black) and as-prepared Nir reduced with excess ascorbate (red) and excess dithionite (blue).[40] The terms "as-prepared", "as-isolated", and "as-purified" refer to protein samples obtained after protein purification, which is usually performed by liquid chromatography (FPLC) under aerobic conditions (*E*~

100-300 mV depending on the protein sample). Both T1 and T2 in their oxidized Cu(II) form ($d^9$, $S$= 1/2) give rise to superposed nearly axial EPR signals distinguishable through their $A_{\|}$ features ( $A_{\|}^{T1} < A_{\|}^{T2}$ ) (Figure 8A, black spectrum, EPR parameters are given in the caption). Upon incubation with sodium ascorbate ($E$ ~ 0 mV), T1 becomes EPR silent as is reduced to Cu(I) ($d^{10}$, $S$= 0), whereas a fraction of T2 remains in the Cu(II) form (Figure 8A, red spectrum). This conclusion is obtained from the doubly integrated EPR spectrum (area under the absorption spectrum), which is proportional to the number of spins (integrated spectrum of ascorbate-reduced Nir is ~ 5 % of that of as-prepared Nir). In contrast, no EPR signals are detected upon addition of a 10-fold molar excess of sodium dithionite under anaerobic conditions ($E$~ -450 mV), indicating that both copper centers are reduced (Figure 8A, blue spectrum). Ferricyanide addition to as-prepared Nir ($E$ ~ 400 mV) does not modify the intensity and line shape of the EPR signal, which indicates that both copper centers are completely oxidized in the as-prepared form of the protein. All these findings indicate that the T1 reduction potential is higher than that of T2, and that the reduction potentials of both centers fall in the range +400 to 0 mV.[41] The analysis of the red spectrum in Figure 8A is trivial as the ascorbate-reduced sample shows only the T2 signal, while that of the black spectrum (as-prepared Nir) is more difficult as both T1 and T2 signals are superposed. The procedure followed to perform simulations of superposed EPR signals implies to simulate each spectral component separately, to normalize them, and then to add these simulated components in different ratios until the best agreement between simulation and experiment is achieved. EPR analysis by simulation of as-prepared Nir spectrum indicates a 1:1 ratio for T1:T2, in line with metal analysis (2 Cu atoms *per* protein monomer), and since no important modifications are observed for T1 and T2 EPR spectra, no magnetic coupling can be detected under the experimental conditions of the measurement. EPR parameters for both T1 and T2 centers (see caption to Figure 8A, $g_{\|} > g_{\perp} > 2$) are consistent with a $d_{x^2-y^2}$ ground state.

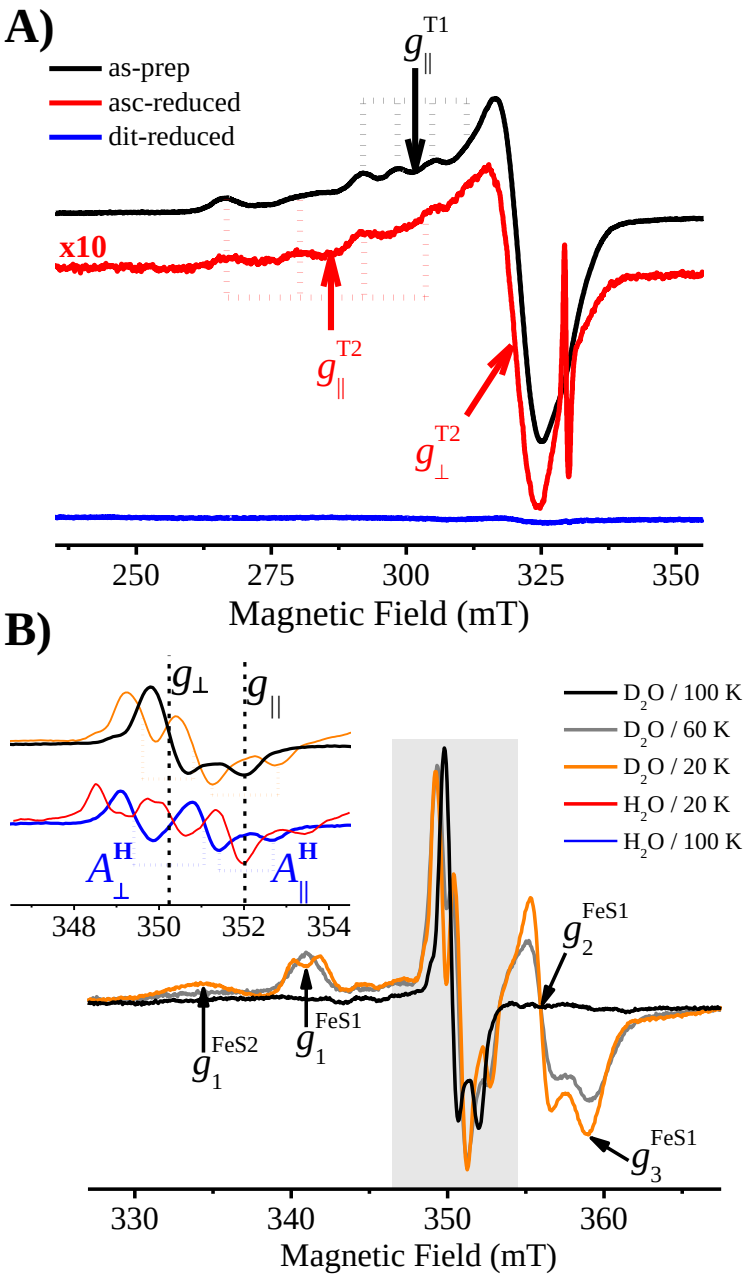


Figure 8. **A)** X-band EPR spectra of copper-containing Nir from *Sinorhizobium meliloti* 2011 obtained under different experimental conditions; as-prep, as-prepared; asc-red, as-prep Nir incubated with sodium ascorbate; dit-red, as-prep Nir incubated with sodium dithionite. The narrow signal at ~ 330 mT corresponds to an EPR-detectable ascorbyl radical. EPR parameters obtained by simulation were $g_{1,2,3}$= 2.190, 2.062, 2.033, $A_1$= 5.8 mT ($59 \times 10^{-4}$ $cm^{-1}$) for T1; $g_{\|,\perp}$= 2.304, 2.053, $A_\|$= 14 mT ($150 \times 10^{-4}$ $cm^{-1}$) for T2.[40] **B)** X-band EPR spectra

of the Mo-containing Aor from *Desulfovibrio gigas* obtained upon dithionite reduction in $^{2}H_2O$-exchanged samples at 100, 60, and 20 K. The gray shadowed region is enlarged in the inset, which shows in addition the spectra at 100 and 20 K in normal water. EPR parameters obtained by simulation were $g_1 \sim g_2 = g_\perp = 1.970$, $g_\parallel = 1.959$, $A^{H}_{1,2=3} = 1.5, 1.6$ mT (14, $15 \times 10^{-4}$ $cm^{-1}$) for Mo, $g_{1,2,3}$=2.023, 1.938, 1.919 for FeS1, and $g_{1,2,3}$= 2.060, 1.979, 1.900 for FeS2. The $g_2$ feature of FeS2 is overlapped with the Mo(V) signal.

In contrast to Nir, Aor develops EPR signals only upon dithionite addition, indicating that the reduction potentials of the metal centers are lower than 0 mV. Before going to the EPR analysis of Aor, just a brief consideration regarding the electronic structure of the Mo and FeS metal centers. The molybdenum atom can be found in three different oxidation states, Mo(VI), Mo(V), and Mo(IV). Only Mo(V) ($d^1$, $S$= 1/2) is detectable by EPR and gives rise to signals with all $g$-values lower than 2. The two [2Fe-2S] centers can be detected in two redox states. The oxidized state ($[2Fe\text{-}2S]^{2+}$) is EPR silent as it contains two strongly antiferromagnetically coupled Fe(III) ions with a ground state with $S$= 0 (section 4.2), which is the only one thermally populated. The $[2Fe\text{-}2S]^{2+}$ center becomes paramagnetic on reduction of one of the Fe(III) ions to Fe(II). The resulting Fe(II)-Fe(III) pair ($[2Fe\text{-}2S]^{1+}$) is also strongly antiferromagnetically coupled, but with an $S$= 1/2 ground state.[42]

Dithionite reduction of Aor for 20 min under anaerobic conditions ($E$ ~ -450 mV *vs* NHE) gives rise to EPR signals associated with the Mo(V) ion and the two $[2Fe\text{-}2S]^{1+}$ clusters (Figure 8B). The Mo(V) signal obtained under these conditions is commonly named “slow” in the literature on Mo-enzymes (black and blue spectra in the inset on Figure 8B),[35a] but hereafter it will be referred to as Mo(V) EPR signal. Whereas ~ 100 % of the FeS centers are paramagnetic at this potential, only about 10 % of the total molybdenum is obtained as Mo(V) species, which can be easily understood taking into account the reduction potentials of the

metal centers ($E°'_{MoVI/V,V/IV}$= -450,-530 mV; $E°'_{FeS1,2}$= -280,-285 mV, values for *D. gigas* Aor).[43] The Mo(V) EPR signal is detected over the whole range of temperature in which Aor is studied (4-150 K). The EPR signal obtained above 90 K shows a nearly axial symmetry with $g_{\perp} > g_{\parallel}$ and hyperfine structure with a species with $I$= 1/2 (Figure 8B, blue spectrum in the inset; EPR parameters are given in the caption). The species with $I$= 1/2 corresponds to a solvent exchangeable proton as demonstrated from the spectrum of Aor in $^{2}H_2O$ (Figure 8B, black spectrum in the inset). Solvent exchange is commonly used in the EPR characterization of metalloproteins to differentiate hyperfine splitting of solvent exchangeable protons associated with metal ligands such as –OH, $H_2O$, and –SH groups from those associated with non-solvent exchangeable protons, such as protons from amino acid residues and/or organic prosthetic groups. In contrast, the EPR signals of FeS1 and FeS2 (Figure 8B, gray and orange spectra) are observed at temperatures below 80 K and 50 K, respectively, indicating that the three centers have different spin-lattice relaxation times ($T_1^{FeS2} < T_1^{FeS1} < T_1^{Mo(V)}$). It is widely known that $T_1$ depends on temperature: the higher the temperature, the shorter the $T_1$ or, equivalently, the higher the relaxation rate. The fact that no FeS EPR signals are detected above 80 K is due to the short $T_1^{FeS}$-values, as the breadth of the EPR resonance line is proportional to $1/T_1$.

The spectra of Figure 8B show also temperature-dependent splitting. This is observed for the Mo(V) signal below 70 K (orange and red spectra in the inset) and for FeS1 below 30 K (orange spectrum), indicating the presence of magnetic couplings between centers. These EPR spectra can be interpreted assuming two independent pairs of $S$= 1/2 centers, Mo(V)-FeS1 and FeS1-FeS2, as both Mo-FeS2 distance (d= 25.6 Å) and chemical path (Figure 7, bottom) are too long to consider magnetic coupling between both centers.[2b] The Mo(V) EPR signal splitting can be analyzed through Equation (2), but not its temperature dependence,

which arises from the different relaxation rates of the interacting centers.[44] The theoretical formalism behind these ideas is briefly outlined in section 6.4.

### 6.3 EPR-monitored Redox Titrations

The understanding at molecular level of the catalytic mechanism of a redox enzyme and its relationship with the intramolecular electron transfer process requires the determination of the reduction potentials of the metal centers situated along the electron transfer chains, *e.g.* T1 and T2 for Nir, and Mo, FeS1, and FeS2 for Aor. The preferred technique to measure reduction potentials is cyclic voltammetry, but when working with metalloproteins some technical problems such as an inefficient electron transfer between the protein and the working electrode and/or a bad resolution of the potential peaks can preclude its use. These problems can alternatively be overcome performing redox titrations monitored by spectroscopic techniques such as EPR. Figure 9 shows the redox potentiometric titration curves of Nir monitored by EPR under anaerobic conditions, together with the EPR spectra at different potentials in the inset on the figure. Different strategies can be used to evaluate the signal intensity associated with each spectral component: i) to simulate the EPR spectra, ii) to evaluate the intensity of non-overlapping features, *e.g.* the non-overlapping features at $g_{\|}$ of Nir (Figure 8A),[41a] iii) to take EPR spectra as a function of temperature (Figure 8B),[44a] or iv) to evaluate the intensity of the more intense spectral peak of overlapped EPR signals, *e.g.* the peak that arises from the sum of the $g_{\perp}$ features of both T1 and T2 centers (Figure 9).[45] The analysis of the data is usually performed assuming independent Nernst equations that are least-squares fit to the data, though in some cases it is necessary to take into consideration cooperative effects between the redox centers.[46]

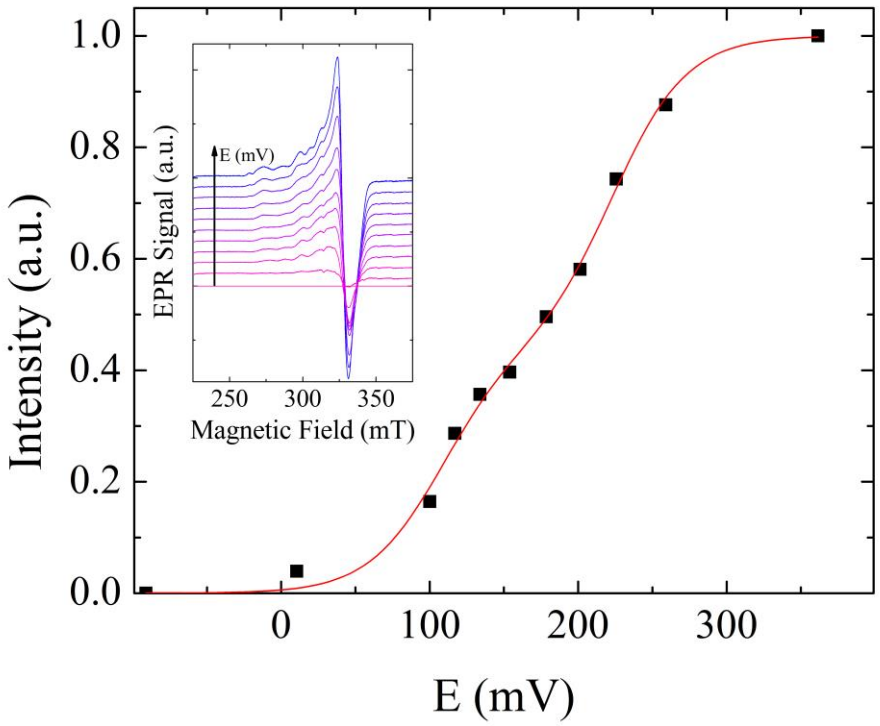


Figure 9. Redox potentiometric titration of Nir monitored by EPR. The red solid line was obtained by least squares fitting a two-independent component Nernst equation with n= 1 to the data. The EPR spectra as a function of the potential are shown in the inset. The reduction potentials were $E^{o\prime}$= 224 ± 4 mV for T1 and $E^{o\prime}$= 108 ± 5 mV for T2.[45]

### 6.4 EPR Assignment of Metal Centers in Macromolecules

The characterization of the electron transfer chains in redox metalloenzymes requires one to assign the spectroscopically detected metal centers to those observed in the X-ray structure. The problem is simple in proteins with metal centers that show distinguishable EPR features, *e.g.* the two Cu centers of Nir, but the solution is not trivial for proteins such as Aor which has two FeS centers that do not show a direct correlation between EPR properties and structure. This problem can be solved using different strategies based on the analysis of the weak magnetic interactions between the redox cofactors.

The analysis of the magnetic coupling between the Mo(V) ion and the proximal FeS center in Aor requires spectral simulation of the split Mo(V) signal taking into account Equation (2). This implies to estimate **g** and **D** eigenvalues and eigenvectors of the interacting centers and the magnitude of *J* (see sections 4.1 and 4.2), which is clearly overparameterized. However, the problem can be simplified assuming that the splitting of the Mo(V) signal is under the condition of weak exchange limit with $J << \Delta B$ (section 4.2 and Figure 3) and that $D_{dip}$ is mainly folded into the linewidth. As the g-values of the Mo(V) center can be obtained independently from other EPR experiment, the only parameter to be determined is the splitting of the Mo(V) signal. Although this approach estimates roughly *J*, it is useful in the assignment of the EPR detectable metal center with those present in the structure of the systems.

One of the strategies to correlate EPR with structural data is based on the comparative analysis of the Mo(V) spectra in Aor samples poised at different potentials, one in which the FeS centers are fully reduced (*E*= - 450 mV) and another in which they are not (*E*= - 334 mV). This strategy can be used when the reduction potentials of the two FeS centers differ by at least ~ 50 mV, as is the case for the FeS centers of Aor from *Desulfovibrio alaskensis* (midpoint redox potentials for FeS1 and FeS2 are -275 mV and -325 mV, respectively). [44a] Figure 10, upper, shows the different Aor microstates that can be obtained at different reduction levels, whereas the lower panel shows the 20 K EPR spectra at -450 mV and -334 mV. At -450 mV, the FeS centers are completely reduced ($[2Fe\text{-}2S]^{+1}$, *S*= 1/2) ($P_{10}$ + $P_{11}$); hence the Mo(V) ion of the $P_{10}$ microstate is magnetically coupled to the closest FeS center yielding a fully split Mo(V) EPR signal (blue spectrum in Figure 10). In contrast, the spectrum at -334 mV results from the superposition of both split ($P_5$ + $P_{10}$) and non-split ($P_1$ + $P_6$) components for the Mo(V) EPR signal. By using the midpoint reduction potential of each FeS center at -334 mV, it is possible to predict the relative probability of finding a given

microstate as a function of the potential and hence the proportion of each component (split and non-split Mo(V) EPR signal) contributing to the EPR signal as a function of the potential.[44a] Simulation sim-a in Figure 10 was obtained assuming that the EPR-detectable FeS1 is the center proximal to the Mo(V) ion, whereas simulation sim-b assuming that FeS2 is the proximal center. A good agreement between simulation and experiment is only obtained for sim-a, confirming that the center giving the FeS1 signal is the cluster proximal to molybdenum.

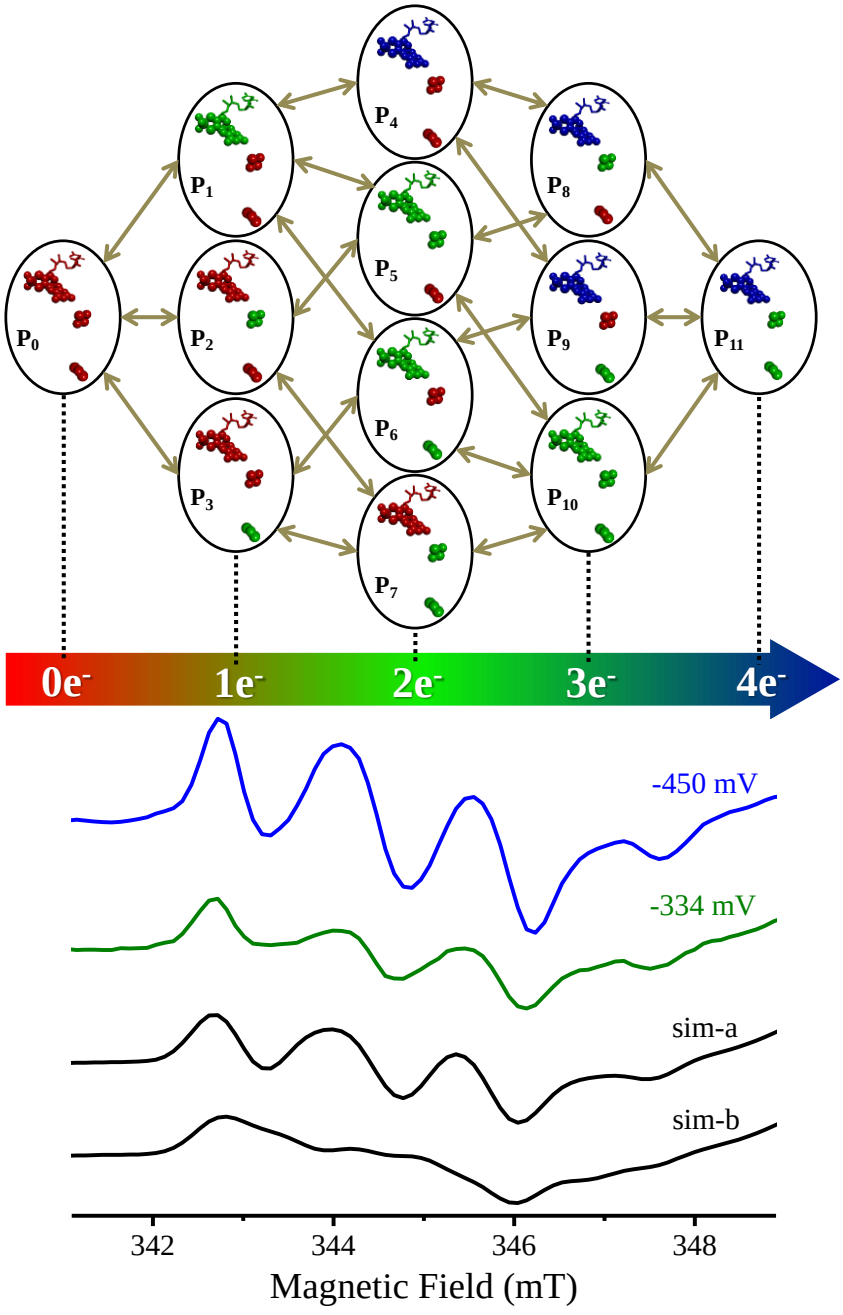

Figure 10. Upper. Schematic representation of the 12 possible microstates in Aor molecules at different reduction levels. Color codes are red for Mo(VI) and oxidized FeS ($[2Fe\text{-}2S]^{+2}$), green for Mo(V) and reduced FeS ($[2Fe\text{-}2S]^{+1}$), and blue for Mo(IV). The double-headed arrows connect microstates separated by one-electron reduction/oxidation ($P_0$ and $P_{11}$ represent the fully oxidized and reduced states, respectively). Lower. Experimental 20 K EPR spectra of Aor samples at -450 and -334 mV. Simulation sim-a was obtained considering that the EPR-identified FeS1 is the center closer to Mo, whereas sim-b was obtained considering that FeS2 is the closer one. EPR parameters for simulation were $g_{1,2,3}$= 1.959,1.969,1.971; $A_{1,2,3}$= 1.6 mT ($15 \times 10^{-4}$ $cm^{-1}$), and $J_{1=2,3}$= 10, $13 \times 10^{-4}$ $cm^{-1}$. The hyperfine coupling $A$ is assigned to a Mo ligand proton ($I$=1/2) and $J_{1,2,3}$ is a matrix associated with the splitting provoked by magnetic coupling between Mo and the proximal FeS center. See text and reference [44a] for details.

Another strategy to assign EPR detectable metal centers with those of the structure consists in the analysis of the split Mo(V) signal as a function of the relaxation time $T_1$ of the interacting FeS center (Figure 11). Left panels show in detail the temperature dependence of the Mo(V) signal in as-prepared (upper) and $^2H_2O$-exchanged (bottom) samples of Aor. The right panels in Figure 11 correspond to EPR simulations obtained with a model based on the density matrix formalism as proposed by Bloch, Wangeness and Redfield (BWR) applied to a dimer of two dissimilar $S$= 1/2 spins.[47] The mathematical formalism employed in the model to simulate the experimental spectra can be found in references [48] and [49].

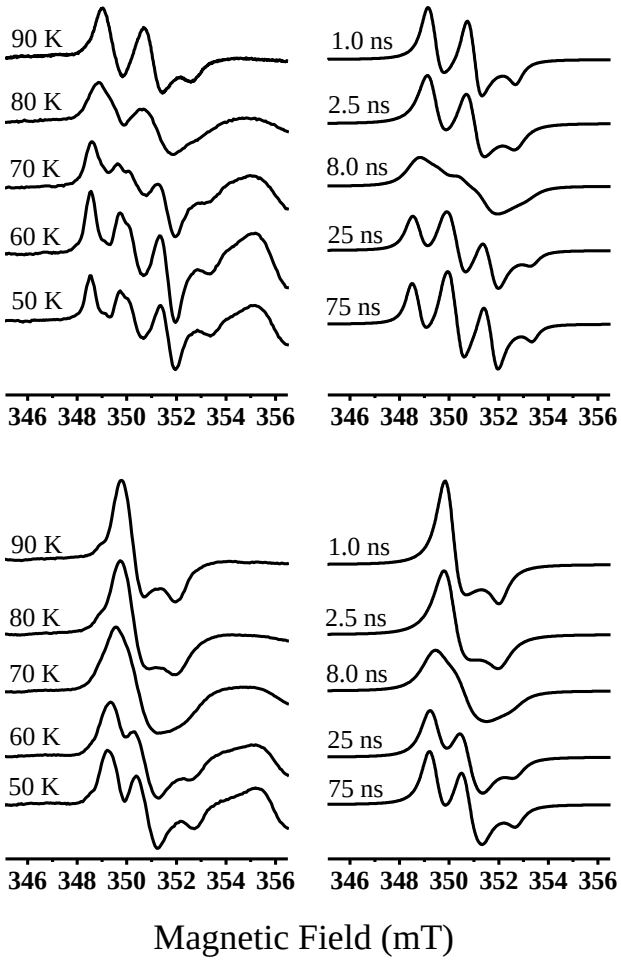


Figure 11. Experimental Mo(V) EPR signals of Aor as a function of temperature (left panel) together with simulation as a function of relaxation times $T_1^{FeS1}$ (right panel). The top and bottom panels correspond to samples in $^1H_2O$ and $^2H_2O$, respectively. Temperatures of the experiment and FeS1 relaxation times for simulation are indicated. The spin Hamiltonian parameters for simulation of Mo(V) signals in $^1H_2O$-exchanged Aor were $g_{1,2,3}$= 1.971, 1.969, 1.959 and $|J| = 1.2 \times 10^{-3}$ cm$^{-1}$ (*D* was considered to be folded into the linewidth for simplicity). Same parameters and $A_{1,2=3}$ = 1.5 mT ($14\times 10^{-4}$ cm$^{-1}$, 1.6 mT ($15 \times 10^{-4}$ cm$^{-1}$) (hyperfine matrix of the solvent exchangeable proton) were used for the as-prepared sample. See reference [49] for details.

By inspecting Figure 11, two well differentiated regimes can be clearly identified at both extremes of the temperature range. At high temperature ($T \geq 90$ K), when FeS1 relaxes extremely fast so that it has a very short relaxation time ($T_1^{FeS1} \leq 1$ ns), the BWR model predicts Mo(V) spectra corresponding to those of an uncoupled system. This means that the fast relaxing center is modulating the interaction between centers in such a way that the effect of the intradimer coupling is averaged to zero. In contrast, at low temperatures ($T \leq 50$ K) when FeS1 center relaxes slowly ($T_1^{FeS1} \geq 75$ ns), no modulation of the intradimer coupling can be detected, and the spectra correspond to those of a coupled system. Intermediate situations with partial collapse and broadening of the Mo(V) resonances are observed between these two limits, which cannot be explained either with Equation (1) or Equation (2).

This assignment methodology consists of performing EPR simulations using relaxation times that can give the best agreement with the experimental spectra. Then, to identify which EPR detectable FeS center is closer to Mo, it is necessary to compare the experimental temperature dependence of $T_1^{FeS1}$ and $T_1^{FeS2}$ with those predicted theoretically by the BWR model. One of the methods that can be utilized to determine the $T_1$-temperature dependence by CW EPR can be found in reference [50]. For Aor, a good matching between experiment and simulation was obtained for $T_1$ associated with the EPR-detected FeS1, indicating that this is the FeS center proximal to the Mo site.

### 6.5 EPR Spectroscopy of Metal Centers Reacted with Exogenous Ligands

EPR spectroscopy also allows one to obtain important structural information about the metal centers as well as to elucidate the inhibition mechanism in metalloenzymes. The formation of a stable complex at the T2 active site in Nir with the substrate and product of the reaction was proved by EPR,[51] which was also crystallographically confirmed.[52] In contrast, no EPR evidences of substrate and product interaction has been reported for Aor, although

EPR studies of Aor with irreversible (*e.g.* arsenite) and reversible (*e.g.* polyalcohols) inhibitors are well documented. [53] EPR experiments performed on dithionite reduced arsenite-inhibited Aor prepared in both $H_2O$ and $^2H_2O$ solvents showed similar results, indicating that the arsenic atom interacts with the molybdenum ion through strong hyperfine and quadrupolar interactions with the As nucleus (Figure 12), [53b, 54] likely through the equatorial $OH_x$ ligand to molybdenum (Figure 7, bottom). This conclusion was also confirmed with X-ray data taken on single crystals of Aor soaked with a buffer containing $NaAsO_2$.[53b, 54] In this structure, the arsenic atom is bound to three oxygen atoms with one of them being in a bridging position between molybdenum and arsenic atoms (Figure 12). Structural results confirm that the nearly square pyramidal coordination of the Mo site is not lost upon arsenite binding, which is in line with the EPR results that shows a nearly axial **g**-matrix.

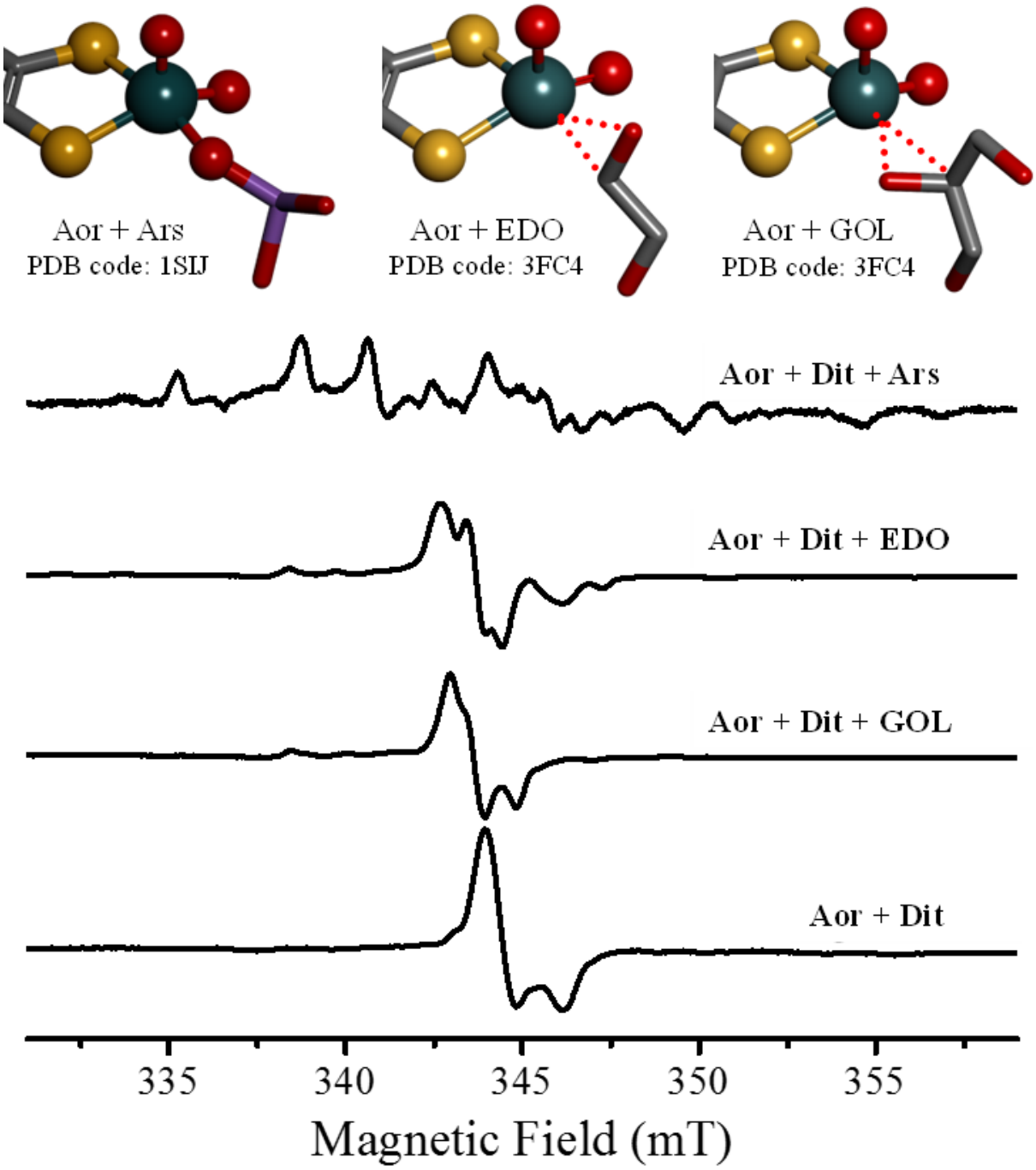


Figure 12. Upper. Coordination around the Mo center determined by X-ray crystallography for arsenite- (Ars), ethylene glycol- (EDO), and glycerol- (GOL) inhibited Aor from *D. gigas*. PDB codes are indicated. Dotted lines indicate interactions between Mo and the inhibitor molecules within bonding distances. Lower. X-band EPR spectra of Aor reacted with these inhibitors at 100 K. The spectrum of dithionite (Dit) reduced as-purified Aor is given for

comparison. EPR parameters were $g_{1,2,3}$= 1.922, 1.979, 1.972, for Ars-reacted Aor; $g_{1,2,3}$= 1.978, 1.972, 1.968 for EDO-reacted Aor; $g_{1,2,3}$= 1.977, 1.973, 1.966 for GOL-reacted Aor.

In contrast to arsenite, ethylene glycol and glycerol are reversible inhibitors of Aor. The EPR spectra of dithionite-reduced Aor samples reacted with either ethylene glycol or glycerol show EPR signals with rhombic symmetry (Figure 12, EPR parameters in the caption to the figure).[53a] The fact that the EPR signals obtained with both alcohols depart considerably from the axial symmetry associated with Mo(V) complexes in square pyramidal coordination suggests a severe distortion of the molybdenum site for both alcohol-inhibited species. A similar conclusion was obtained from X-ray data taken on single crystals of Aor soaked with alcohol-containing buffers, which shows that the nearly square pyramidal coordination of the Mo site is lost upon inhibition (Figure 12, upper panel).[53a]

**6.6 EPR Signal Saturation Studies to Evaluate Integrity of Electron Transfer Pathways**

The integrity of the electron transfer pathway upon enzyme inhibition can also be investigated by EPR saturation studies when one of the paramagnetic centers of a spin pair is redox inert, which is the case of the Mo(V) ion in Aor inhibited with arsenite, ethylene glycol, and glycerol.[53] Figure 13 shows a saturation experiment for the Mo(V) EPR signal at distinct microwave powers (*P*) obtained upon air oxidation of dithionite reduced arsenite-reacted Aor. For low values of *P*, the ratio *I*/sqrt(*P*), where *I* is the intensity of the EPR signal, is constant, indicating no saturation of the EPR signal. For higher *P*, *I*/sqrt(*P*) decreases, indicating signal saturation; the higher the *P*, the higher the saturation.

Air-oxidation of arsenite-reduced samples oxidizes the FeS clusters to a diamagnetic state ($[2Fe\text{-}2S]^{+2}$) but leaves the arsenite-reacted molybdenum as Mo(V). Thus, one can evaluate the intensity of the Mo(V) EPR signal in two redox forms of the enzyme, one showing Mo-FeS1 magnetic coupling (reduced sample) and another with no magnetic

coupling (air oxidized). The fact that the reduced sample requires higher *P* to reach the saturation state is due to the fast relaxing FeS1 center that enhances the relaxation rate of the Mo(V) ion, which is provoked by the Mo-FeS1 exchange interaction. This result indicates that the Mo-FeS1 electron transfer pathway can transmit magnetic interaction in the enzyme inhibited form, confirming that the electron transfer pathway is not affected upon inhibition.

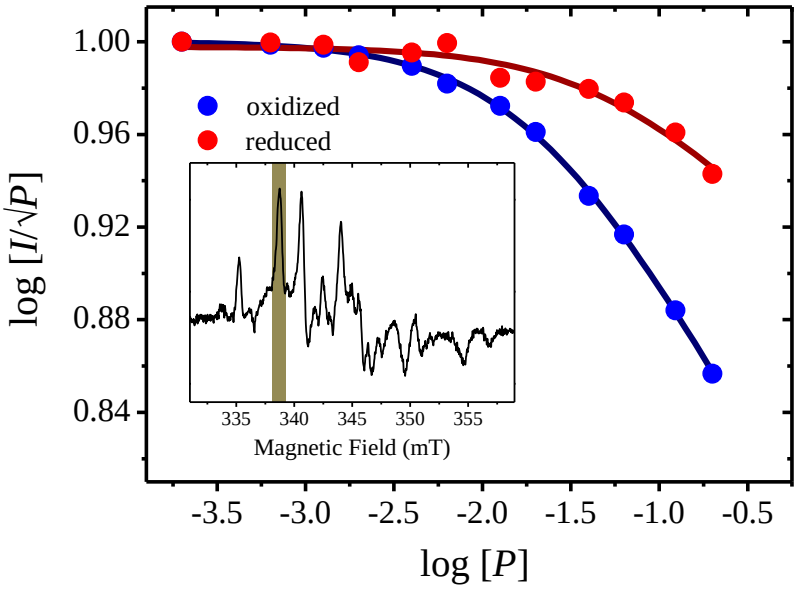


Figure 13. Normalized microwave power dependence plot of reduced (red) and air oxidized (blue) arsenite-inhibited Aor EPR signal. *I*, EPR signal intensity; *P*, microwave power in W. The equation $y= P_1-(P_2/2)\log(1+P/P_3)$ was least squares fitted to the data. $P_1$ is proportional to the EPR line intensity under non-saturating conditions, $P_2$ is related to the EPR linewidth, and $P_3$ is the microwave power for which the saturation factor is one half. [53b, 54-55] The EPR signal peak used to evaluate *I* is shadow in the inset on the figure.

### 6.7 Exchange Interaction and its Relationship with Electron Transfer Processes

Electron transfer processes through long distances between two redox centers in proteins can be studied through the Marcus´ theory, in which the electron transfer rate $k_{et}$ is given by[56]

$$k_{et}= (2\pi/\hbar)(4\pi\lambda kT)^{-1/2}T_{DA}^{2} \exp -(-\Delta G°-\lambda)^2/4\lambda kT \qquad (5)$$

where $-\Delta G^{\circ} = zF\Delta E^{\circ\prime}$ is the driving force of the electron transfer process and is related to the electric potential gradient ($\Delta E^{o\prime}$) between the electron donor D (*e.g.* Mo in Aor and T1 in Nir, Figure 7) and the electron acceptor A (*e.g.* FeS1 in Aor and T2 in Nir), λ is the nuclear energy reorganization parameter, $T_{DA}$ is related to the electronic coupling between A and D, and the other symbols have the usual meaning. The term $T_{DA}$ depends on the topology of the chemical pathway in the protein structure,[57] with $T_{DA}^2$ being proportional to the isotropic exchange constant *J* between D and A under the condition of maximal electron transfer rate ($-\Delta G^{\circ} = \lambda$).[58] Equation 5 shows clearly the relationship between *J* and $k_{et}$ through $T_{DA}$ when the electron transfer reaction is carried out through the chemical pathway associated with *J*.

As EPR is the spectroscopic method of choice to evaluate very weak isotropic exchange constants, it becomes a useful technique to study electron transfer processes in redox proteins presenting exchange coupled centers. Aor is a representative example in which evaluation of *J* can be useful to study the factors that govern electron transfer between redox centers in metalloproteins. The catalytic mechanism of Aor involves substrate binding followed by a two-electron oxidation of the reduced Mo center once the product is released.[39a] The electron-transfer reaction between Mo and FeS1 must be mediated necessarily by the pyranopterin moiety, which functions as an electron transfer conduit during the concerted Mo reoxidation and product exit. The structure of as-purified Aor corresponds to the ready enzyme state that starts the catalytic cycle (Figure 7, bottom), whereas that of alcohol inhibited Aor resembles the situation when the product is formed and remains within bonding distance with the Mo ion (Figure 12, upper). Thus, the evaluation of *J* in these enzyme variants may give information about the molecular processes that occur during the catalytic mechanism.

The evaluation of *J* for the Mo-FeS1 pair requires numerical simulations of the experimental spectra (Figure 8B) with Equation (2). However, as anticipated above in section

6.4, simulations require to determine a large number of parameters, which are normally unknown, but that can be assumed on the basis of distinct types of arguments. Firstly, for long intercenter distances **D** may be assumed to be determined by dipole-dipole interaction and antisymmetric exchange can be ignored because of the low *J* value.[20] The **g**-matrices for the two centers can be evaluated by simulation of the high temperature powder-like spectra (Figure 8B), but not the eigenvectors, which would require a single crystal EPR experiment. When this information is unknown, as is the case for Aor, the eigenvectors of the Mo(V) and FeS1 **g**-matrices can be proposed on the basis of symmetry arguments described in section 4.1. Details on how to perform this type of calculation can be found in references [6e] and [59]. Simulation results (red spectra in Figure 14) show that the FeS1-Mo(V) exchange interaction *J* increases ≈ 2 times in the EDO- and GOL-reacted samples relative to that determined for the dithionite reduced as-prepared sample, which would suggest that the electron transfer pathway is modified upon inhibition.

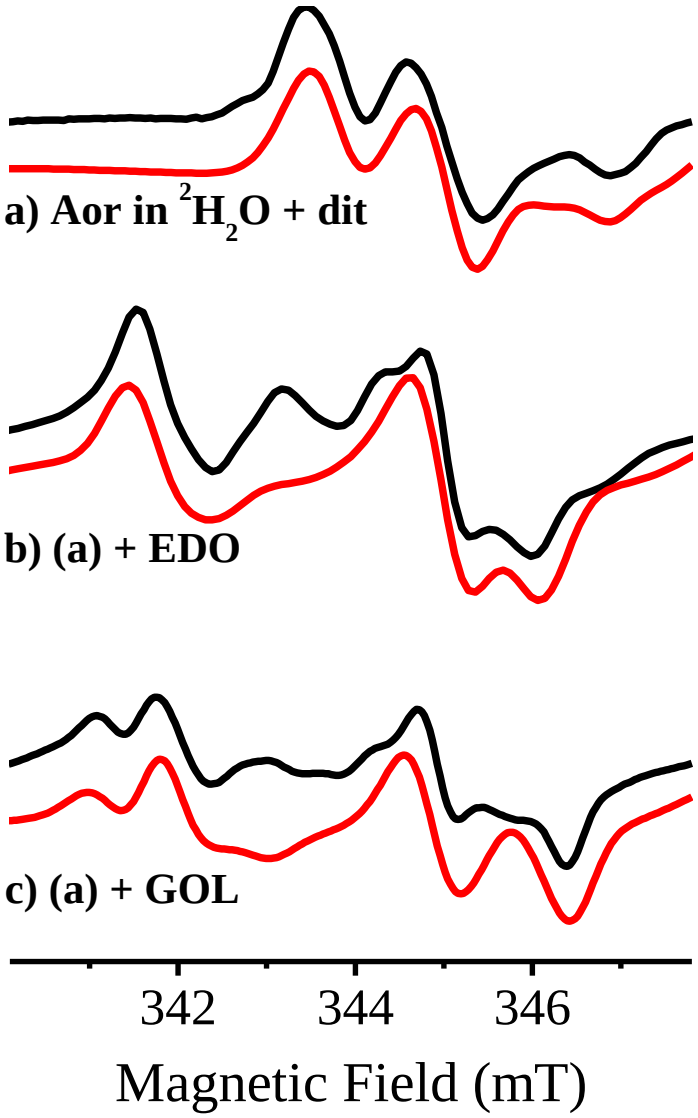


Figure 14. EPR spectra at 20 K of the Mo(V) center together with simulations obtained using Equation (2). a) dithionite (dit) reduced $^2H_2O$-exchanged Aor ($\nu$= 9.64 GHz), b) EDO-reacted Aor, and c) GOL-reacted Aor (both at $\nu$= 9.49 GHz). The three simulations were performed using the same **D**-matrix ($D_{x=y}$= 3.98 × $10^{-4}$ $cm^{-1}$ and $D_z$= -7.96 × $10^{-4}$ $cm^{-1}$) and $J$ = -16.6 × $10^{-4}$ $cm^{-1}$ in spectrum a, and $J$ = 33.3 × $10^{-4}$ $cm^{-1}$ in spectra b and c. The remaining EPR parameters and simulation details can be found in reference [6e].

The fact that $J$ increases ~ 2 times upon alcohol inhibition suggests that the electron transfer mediated by the Mo-FeS1 chemical pathway is enhanced under these conditions. At

this point one should wonder if the changes in *J* are a consequence of structural changes in the pyranopterin electron transfer pathway, or changes in the electronic structure of either Mo(V) or FeS1 centers. Both EPR and structural data show that chemical pathways in as-purified and inhibitor-reacted Aor are essentially identical, confirming that the changes in *J* observed upon inhibition cannot be ascribed to structural changes associated either with pterin and FeS1 or with changes in the electronic structure of FeS1, as its EPR properties remain unchanged upon inhibition.[53a] Therefore, the changes in *J* detected by EPR indicate changes in the electronic structure of Mo(V), a fact that was addressed by computational calculations that showed changes in the catalytically labile site spin density, which is redistributed principally on the Mo(V) atom and partly on the remaining Mo(V) ligands upon alcohol inhibition. [6e] This confirms that the changes in the Mo site electronic structure increases the Mo(V)-FeS1 exchange coupling constant, and that the intraenzyme electron transfer process should be regulated by the catalytic labile $OH_x$ ligand of molybdenum.

## 7. Summary and Outlook

This microreview summarizes the use of CW EPR in the characterization of distinct types of systems of biological interest. The examples presented above have been selected to show how CW EPR can be used to characterize paramagnetic transition metal ion-containing systems such as low molecular weight inorganic complexes and metalloproteins. Although the methodologies used to study both types of systems are in general rather different, we have presented in this paper a unified view of the problem to show that the expertise in the study of inorganic metal complexes can be extended to the characterization of more complex macromolecules and *vice versa*.

From the above sections it is clear that CW EPR is a valuable spectroscopic tool to study not only the geometric and electronic structure of individual paramagnetic transition

metal ions but also to detect and to evaluate very weak isotropic exchange interactions between metal centers, which, from our point of view, is the less exploited field in EPR. Future challenges are evidently related in using the information gathered from the study of both magnetically diluted and undiluted systems in areas such as structural biology, biophysicalchemistry, and sustainable chemistry, where EPR can provide valuable and fine structural information that complements data from conventional X-ray diffraction techniques, and also help in the characterization of intermediates in reactions catalyzed by biomimetic systems and enzymes. Although more sophisticated techniques such as multidimensional and multifrequency pulsed EPR could also be needed to reach the above mentioned goals, CW EPR is still, in our opinion, a very powerful technique and an obligatory step in the study of systems of biological interest containing paramagnetic centers.

**Acknowledgments**

We thank FONCyT, CONICET, and CAI+D-UNL for financial support. We thank R. Calvo, M. C. G. Passeggi, and J. J. G. Moura for fruitful discussions, and three anonymous reviewers for their valuable comments, suggestions, and corrections. We also thank J. J. G. Moura from Department of Chemistry at Universidade Nova de Lisboa for facilitating Aor EPR data. N.I.N., P.J.G, and C.D.B are members of CONICET (Argentina).

**Keywords**

EPR, metal complexes, exchange, metalloproteins

## References


[1] a)J. R. Pilbrow, *Transition Ion Electron Paramagnetic Resonance*, First ed., Oxford University Press, New York, **1990**; b)J. A. Weil, Bolton, J. R., *Electron Paramagnetic Resonance*, 2nd ed., John Wiley & Sons, Hoboken, New Jersey, **2007**; c)A. Carrington, A. D. McLachlan, *Introduction to magnetic resonance with applications to chemistry and chemical physics*, Harper & Row, New York,, **1967**; d)P. H. Rieger, *Electron spin resonance: analysis and interpretation*, Royal Society of Chemistry, **2007**; e)G. Hanson, L. Berliner, *High resolution EPR: applications to metalloenzymes and metals in medicine, Vol. 28*, Springer Science & Business Media, **2009**; f)M. Brustolon, E. Giamello, *Electron paramagnetic resonance: a practitioner's toolkit*, John Wiley & Sons, **2009**; g)W. R. Hagen, *Biomolecular EPR spectroscopy*, CRC press, Boca Raton, FL, **2008**; h)A. Lund, S. Shimada, M. Shiotani, *Principles and applications of ESR spectroscopy*, Springer Science & Business Media, **2011**; i)M. Drescher, G. Jeschke, *EPR spectroscopy: applications in chemistry and biology, Vol. 321*, Springer Science & Business Media, **2012**; j)F. E. Mabbs, D. Collison, *Electron paramagnetic resonance of d transition metal compounds*, Elsevier, **1992**.

[2] a)R. Calvo, *Appl. Magn. Reson.* **2007**, *31*, 271-299; b)S. K. Hoffmann, W. Hilczer, J. Goslar, *Appl. Magn. Reson.* **1994**, *7*, 289-321; c)M. Chiesa, E. Giamello, M. Che, *Chem. Rev.* **2010**, *110*, 1320-1347; d)J. Krzystek, A. Ozarowski, J. Telser, *Coord. Chem. Rev.* **2006**, *250*, 2308-2324; e)D. Gatteschi, A. L. Barra, A. Caneschi, A. Cornia, R. Sessoli, L. Sorace, *Coord. Chem. Rev.* **2006**, *250*, 1514-1529; f)T. Prisner, M. Rohrer, F. MacMillan, *Annu. Rev. Phys. Chem.* **2001**, *52*, 279-313; g)P. C. Riedi, G. M. Smith, *Electron paramagnetic resonance* **2002**, *18*, 254-303; h)S. Van Doorslaer, F. Desmet, in *Methods in Enzymology, Vol. 437*, **2008**, pp. 287-310; i)J. Krzystek, A. Ozarowski, J. Telser, D. C. Crans, *Coord. Chem. Rev.* **2015**, *301–302*, 123-133.

[3] a)O. Kahn, *Molecular Magnetism*, VCH Publishers New York, **1993**; b)A. Bencini, Gatteschi, D., *Electron Paramagnetic Resonance of Exchange Coupled Systems*, Springer-Verlag, Berlin, Germany, **1990**; c)D. Gatteschi, *Adv. Mater.* **1994**, *6*, 635-645; d)J. Mroziński, *Coord. Chem. Rev.* **2005**, *249*, 2534-2548.

[4] a)O. Kahn, *Angew. Chem. Int. Ed. Engl.* **1985**, *24*, 834-850; b)M. Atzori, A. Serpe, P. Deplano, J. A. Schlueter, M. Laura Mercuri, *Inorg. Chem. Front.* **2015**, *2*, 108-115.

[5] a)M. Castellano, R. Ruiz-García, J. Cano, J. Ferrando-Soria, E. Pardo, F. R. Fortea-Pérez, S. E. Stiriba, M. Julve, F. Lloret, *Acc. Chem. Res.* **2015**, *48*, 510-520; b)F. Meyer, S. Demeshko, G. Leibeling, B. Kersting, E. Kaifer, H. Pritzkow, *Chem. Eur. J.* **2005**, *11*, 1518-1526; c)E. Moreno Pineda, N. F. Chilton, R. Marx, M. Dörfel, D. O. Sells, P. Neugebauer, S.-D. Jiang, D. Collison, J. van Slageren, E. J. L. McInnes, R. E. P. Winpenny, *Nat. Commun.* **2014**, *5*, 5243; d)J. Camarero, E. Coronado, *J. Mater. Chem.* **2009**, *19*, 1678-1684; e)D. Cangussu, E. Pardo, M.-C. Dul, R. Lescouëzec, P. Herson, Y. Journaux, E. F. Pedroso, C. L. M. Pereira, H. O. Stumpf, M. Carmen Muñoz, R. Ruiz-García, J. Cano, M. Julve, F. Lloret, *Inorg. Chim. Acta* **2008**, *361*, 3394-3402.

[6] a)A. V. Astashkin, B. O. Elmore, W. Fan, J. G. Guillemette, C. Feng, *J. Am. Chem. Soc.* **2010**, *132*, 12059-12067; b)A. K. Upadhyay, D. T. Petasis, D. M. Arciero, A. B. Hooper, M. P. Hendrich, *J. Am. Chem. Soc.* **2003**, *125*, 1738-1747; c)C. D. Brondino, M. G. Rivas, M. J. Romão, J. J. G. Moura, I. Moura, *Acc. Chem. Res.* **2006**, *39*, 788-796; d)J. H. Van Wonderen, V. S. Oganesyan, N. J. Watmough, D. J. Richardson, A. J. Thomson, M. R. Cheesman, *Biochem. J.* **2013**, *451*, 389-394; e)M. Gómez, N.

Neuman, S. Dalosto, P. González, J. G. Moura, A. Rizzi, C. Brondino, *J. Biol. Inorg. Chem.* **2015**, *20*, 233-242.

[7] a)J. M. Schveigkardt, A. C. Rizzi, O. E. Piro, E. E. Castellano, R. Costa de Santana, R. Calvo, C. D. Brondino, *Eur. J. Inorg. Chem.* **2002**, 2913-2919; b)B. K. Maiti, L. B. Maia, K. Pal, B. Pakhira, T. Avilés, I. Moura, S. R. Pauleta, J. L. Nuñez, A. C. Rizzi, C. D. Brondino, S. Sarkar, J. J. G. Moura, *Inorg. Chem.* **2014**, *53*, 12799-12808; c)M. van Gastel, M. J. Boulanger, G. W. Canters, M. Huber, M. E. P. Murphy, M. P. Verbeet, E. J. J. Groenen, *J. Phys. Chem. B* **2001**, *105*, 2236-2243.

[8] a)D. R. Boer, A. Thapper, C. D. Brondino, M. J. Romão, J. J. G. Moura, *Journal of the American Chemical Society* **2004**, *126*, 8614-8615; b)E. P. Duliba, E. G. Seebauer, R. Linn Belford, *J. Magn. Reson.* **1982**, *49*, 507-516.

[9] M. M. Cosper, F. Neese, A. V. Astashkin, M. D. Carducci, A. M. Raitsimring, J. H. Enemark, *Inorg. Chem.* **2005**, *44*, 1290-1301.

[10] a)A. C. Rizzi, C. D. Brondino, R. Calvo, R. Baggio, M. T. Garland, R. E. Rapp, *Inorg. Chem.* **2003**, *42*, 4409-4416; b)D. Maganas, S. Milikisyants, J. M. A. Rijnbeek, S. Sottini, N. Levesanos, P. Kyritsis, E. J. J. Groenen, *Inorg. Chem.* **2010**, *49*, 595-605; c)V. Rosa, P. J. Gonzalez, T. Avilés, P. T. Gomes, R. Welter, A. C. Rizzi, M. C. Passeggi, C. D. Brondino, *Eur. J. Inorg. Chem.* **2006**, 4761-4769.

[11] a)N. I. Neuman, E. Winkler, O. Peña, M. C. G. Passeggi, A. C. Rizzi, C. D. Brondino, *Inorg. Chem.* **2014**, *53*, 2535-2544; b)A. Bencini, C. Benelli, D. Gatteschi, C. Zanchini, *Inorg. Chem.* **1979**, *18*, 2137-2140.

[12] D. V. J. Hoffman B M, Doan P E, Gurbiel R J, Houseman A L P, Telser J, in *Biological magnetic resonance*, Plenum Press, New York, **1993**, pp. 151-218.

[13] J. Peisach, W. E. Blumberg, *Arch. Biochem. Biophys.* **1974**, *165*, 691-708.

[14] K. Wüthrich, *Helv. Chim. Acta* **1965**, *48*, 779-790.

[15] N. D. Chasteen, in *Biological Magnetic Resonance* (Eds.: L. Berliner, J. Reuben), Springer US, **1981**, pp. 53-119.

[16] G. Barr-David, M. Charara, R. Codd, R. P. Farrell, J. A. Irwin, P. A. Lay, R. Bramley, S. Brumby, J.-Y. Ji, G. R. Hanson, *J. Chem. Soc., Faraday Trans.* **1995**, *91*, 1207-1216.

[17] E. I. Solomon, U. M. Sundaram, T. E. Machonkin, *Chem. Rev.* **1996**, *96*, 2563-2606.

[18] A. Abragam, B. Bleaney, *Electron paramagnetic resonance of transition ions*, Dover Publications, New York, **1986**.

[19] a)R. F. Schlam, M. Perec, R. Calvo, L. Lezama, M. Insausti, T. Rojo, B. M. Foxman, *Inorg. Chim. Acta* **2000**, *310*, 81-88; b)A. Ozarowski, *Inorg. Chem.* **2008**, *47*, 9760-9762; c)L. Gasque, V. M. Ugalde-Saldívar, I. Membrillo, J. Olguín, E. Mijangos, S. Bernès, I. González, *J. Inorg. Biochem.* **2008**, *102*, 1227-1235; d)C. J. Williams, H. Morris, J. Svorec, M. Valková, M. Valko, J. Moncol, M. Mazur, F. Valach, M. Melnik, *J. Mol. Struct.* **2003**, *659*, 53-60.

[20] T. D. Smith, J. R. Pilbrow, *Coord. Chem. Rev.* **1974**, *13*, 173-278.

[21] G. R. Hanson, K. E. Gates, C. J. Noble, M. Griffin, A. Mitchell, S. Benson, *J. Inorg. Biochem.* **2004**, *98*, 903-916.

[22] H. J. Hogben, M. Krzystyniak, G. T. P. Charnock, P. J. Hore, I. Kuprov, *J. Mag. Reson.* **2011**, *208*, 179-194.

[23] S. Stoll, A. Schweiger, *J. Magn. Reson.* **2006**, *178*, 42-55.

[24] a)S. Signorella, C. Hureau, *Coord. Chem. Rev.* **2012**, *256*, 1229-1245; b)F. Yu, J. E. Penner-Hahn, V. L. Pecoraro, *J. Am. Chem. Soc.* **2013**, *135*, 18096-18107; c)F. Thomas, *Eur. J. Inorg. Chem.* **2007**, *2007*, 2379-2404; d)F. G. Mutti, G. Zoppellaro, M. Gullotti, L. Santagostini, R. Pagliarin, K. K. Andersson, L. Casella, *Eur. J. Inorg. Chem.* **2009**, *2009*, 554-566.

[25] C. D. Brondino, N. M. C. Casado, M. C. G. Passeggi, R. Calvo, *Inorg. Chem.* **1993**, *32*, 2078-2084.
[26] P. W. Anderson, P. R. Weiss, *Rev. Mod. Phys.* **1953**, *25*, 269-276.
[27] a)S. M. Avdoshenko, I. N. Ioffe, G. Cuniberti, L. Dunsch, A. A. Popov, *ACS Nano* **2011**, *5*, 9939-9949; b)M. Urdampilleta, N.-V. Nguyen, J.-P. Cleuziou, S. Klyatskaya, M. Ruben, W. Wernsdorfer, *Int. J. Mol. Sci.* **2011**, *12*, 6656; c)M. Urdampilleta, S. Klayatskaya, M. Ruben, W. Wernsdorfer, *ACS Nano* **2015**, *9*, 4458-4464; d)W. Wernsdorfer, N. Aliaga-Alcalde, D. N. Hendrickson, G. Christou, *Nature* **2002**, *416*, 406-409; e)R. Calvo, M. C. Passeggi, R. A. Isaacson, M. Y. Okamura, G. Feher, *Biophys. J.* **1990**, *58*, 149-165.
[28] a)P. W. Anderson, *J. Phys. Soc. Jpn.* **1954**, *9*, 316-339; b)R. A. Sack, *Mol. Phys.* **1958**, *1*, 163-167.
[29] C. D. Brondino, R. Calvo, A. M. Atria, E. Spodine, O. R. Nascimento, O. Peña, *Inorg. Chem.* **1997**, *36*, 3183-3189.
[30] a)N. I. Neuman, V. G. Franco, F. M. Ferroni, R. Baggio, M. C. G. Passeggi, A. C. Rizzi, C. D. Brondino, *J. Phys. Chem. A* **2012**, *116*, 12314-12320; b)N. I. Neuman, M. Perec, P. J. González, M. C. G. Passeggi, A. C. Rizzi, C. D. Brondino, *J. Phys. Chem. A* **2010**, *114*, 13069-13075; c)N. I. Neuman, E. Burna, R. Baggio, M. C. G. Passeggi, A. C. Rizzi, C. D. Brondino, *Inorg. Chem. Front.* **2015**, *2*, 837-845.
[31] a)C. D. Brondino, R. Calvo, E. J. Baran, *Chem. Phys. Lett.* **1997**, *271*, 51-54; b)R. Calvo, J. E. Abud, R. P. Sartoris, R. C. Santana, *Phys. Rev. B.* **2011**, *84*, 104433-104445; c)R. P. Sartoris, O. R. Nascimento, R. C. Santana, M. Perec, R. F. Baggio, R. Calvo, *Dalton Trans.* **2015**, *44*, 4732-4743.
[32] Y.-Q. Zheng, H.-Z. Xie, *J. Sol. State Chem.* **2004**, *177*, 1352-1358.
[33] J. J. R. F. d. Silva, R. J. P. Williams, *The biological chemistry of the elements : the inorganic chemistry of life*, Clarendon Press, Oxford, **1991**.
[34] C. Andreini, I. Bertini, G. Cavallaro, G. Holliday, J. Thornton, *J. Biol. Inorg. Chem.* **2008**, *13*, 1205-1218.
[35] a)R. Hille, *Chem. Rev.* **1996**, *96*, 2757-2816; b)W. G. Zumft, *Microbiol. Mol. Biol. Rev.* **1997**, *61*, 533-616.
[36] a)J. W. Godden, S. Turley, D. C. Teller, E. T. Adman, M. Y. Liu, W. J. Payne, J. LeGall, *Science* **1991**, *253*, 438-442; b)M. Kukimoto, M. Nishiyama, M. E. P. Murphy, S. Turley, E. T. Adman, S. Horinouchi, T. Beppu, *Biochemistry* **1994**, *33*, 5246-5252; c)T. Inoue, M. Gotowda, Deligeer, K. Kataoka, K. Yamaguchi, S. Suzuki, H. Watanabe, M. Gohow, Y. Kai, *J. Biochem.* **1998**, *124*, 876-879.
[37] a)F. E. Dodd, J. Van Beeumen, R. R. Eady, S. S. Hasnain, *J. Mol. Biol.* **1998**, *282*, 369-382; b)S. Suzuki, T. Kohzuma, Deligeer, K. Yamaguchi, N. Nakamura, S. Shidara, K. Kobayashi, S. Tagawa, *J. Am. Chem. Soc.* **1994**, *116*, 11145-11146; c)E. Libby, B. A. Averill, *Biochem. Biophys. Res. Commun.* **1992**, *187*, 1529-1535.
[38] a)M. J. Romao, M. Archer, I. Moura, J. J. Moura, J. LeGall, R. Engh, M. Schneider, P. Hof, R. Huber, *Science* **1995**, *270*, 1170-1176; b)J. M. Rebelo, J. M. Dias, R. Huber, J. J. Moura, M. J. Romao, *J. Biol. Inorg. Chem.* **2001**, *6*, 791-800.
[39] a)C. D. Brondino, M. G. Rivas, M. J. Romao, J. J. Moura, I. Moura, *Acc. Chem. Res.* **2006**, *39*, 788-796; b)L. Krippahl, P. N. Palma, I. Moura, J. J. G. Moura, *Eur. J. Inorg. Chem.* **2006**, 3835-3840.
[40] F. M. Ferroni, S. A. Guerrero, A. C. Rizzi, C. D. Brondino, *J. Inorg. Biochem.* **2012**, *114*, 8-14.
[41] a)D. Pinho, S. Besson, C. D. Brondino, B. de Castro, I. Moura, *Eur. J. Biochem.* **2004**, *271*, 2361-2369; b)K. Olesen, A. Veselov, Y. Zhao, Y. Wang, B. Danner, C. P. Scholes, J. P. Shapleigh, *Biochemistry* **1998**, *37*, 6086-6094.

[42] M. K. Johnson, *Curr. Opin. Chem. Biol.* **1998**, *2*, 173-181.
[43] J. J. Moura, A. V. Xavier, R. Cammack, D. O. Hall, M. Bruschi, J. Le Gall, *Biochem. J.* **1978**, *173*, 419-425.
[44] a)S. L. Andrade, C. D. Brondino, M. J. Feio, I. Moura, J. J. Moura, *Eur. J. Biochem.* **2000**, *267*, 2054-2061; b)J. Caldeira, V. Belle, M. Asso, B. Guigliarelli, I. Moura, J. J. Moura, P. Bertrand, *Biochemistry* **2000**, *39*, 2700-2707; c)C. More, M. Asso, G. Roger, B. Guigliarelli, J. Caldeira, J. Moura, P. Bertrand, *Biochemistry* **2005**, *44*, 11628-11635.
[45] F. Ferroni, J. Marangon, N. Neuman, J. Cristaldi, S. Brambilla, S. Guerrero, M. Rivas, A. Rizzi, C. Brondino, *J. Biol. Inorg. Chem.* **2014**, *19*, 913-921.
[46] H. E. M. Christensen, I. Coutinho, L. S. Conrad, J. M. Hammerstad-Pedersen, G. Iversen, M. H. Jensen, J. J. Karlsson, J. Ulstrup, A. V. Xavier, *J. Photochem. Photobiol. A* **1994**, *82*, 103-115.
[47] N. M. Atherton, *Electron spin resonance; theory and applications*, Chichester [Eng.] E. Horwood; New York, Halsted Press, **1973**.
[48] K. M. Salikhov, R. T. Galeev, V. K. Voronkova, Y. V. Yablokov, J. Legendziewicz, *App. Mag. Res.* **1998**, *14*, 457-472.
[49] P. J. González, G. I. Barrera, A. C. Rizzi, J. J. G. Moura, M. C. G. Passeggi, C. D. Brondino, *J. Inorg. Biochem.* **2009**, *103*, 1342-1346.
[50] P. Bertrand, G. Roger, J.-P. Gayda, *J. Mag. Res.* **1980**, *40*, 539-549.
[51] A. Veselov, K. Olesen, A. Sienkiewicz, J. P. Shapleigh, C. P. Scholes, *Biochemistry* **1998**, *37*, 6095-6105.
[52] E. I. Tocheva, F. I. Rosell, A. G. Mauk, M. E. P. Murphy, *Science* **2004**, *304*, 867-870.
[53] a)T. Santos-Silva, F. Ferroni, A. Thapper, J. Marangon, P. J. González, A. C. Rizzi, I. Moura, J. J. G. Moura, M. J. Romão, C. D. Brondino, *J. Am. Chem. Soc.* **2009**, *131*, 7990-7998; b)D. R. Boer, A. Thapper, C. D. Brondino, M. J. Romao, J. J. Moura, *J. Am. Chem. Soc.* **2004**, *126*, 8614-8615.
[54] A. Thapper, D. R. Boer, C. D. Brondino, J. J. Moura, M. J. Romao, *J. Biol. Inorg. Chem.* **2007**, *12*, 353-366.
[55] M. W. Makinen, L. C. Kuo, M. B. Yim, G. B. Wells, J. M. Fukuyama, J. E. Kim, *J. Am. Chem. Soc.* **1985**, *107*, 5245-5255.
[56] R. A. Marcus, N. Sutin, *Biochim. Biophys. Acta- Reviews on Bioenergetics* **1985**, *811*, 265-322.
[57] J. R. Winkler, H. B. Gray, *J. Biol. Inorg. Chem.* **1997**, *2*, 399-404.
[58] a)R. Calvo, R. A. Isaacson, M. L. Paddock, E. C. Abresch, M. Y. Okamura, A. L. Maniero, L. C. Brunel, G. Feher, *J. Phys. Chem. B.* **2001**, *105*, 4053-4057; b)D. DeVault, *Quantum-mechanical tunnelling in biological systems*, 2nd ed., Cambridge University Press, Cambridge [Cambridgeshire] ; New York, **1984**.
[59] P. Bertrand, P. Camensuli, C. More, B. Guigliarelli, *J. Am. Chem. Soc.* **1996**, *118*, 1426-1434.